BACTERIAL INFECTIONS

The small-molecule SMARt751 reverses *Mycobacterium tuberculosis* resistance to ethionamide in acute and chronic mouse models of tuberculosis

Marion Flipo[1]†, Rosangela Frita[2]†, Marilyne Bourotte[1,3], María S. Martínez-Martínez[4], Markus Boesche[5], Gary W. Boyle[6], Geo Derimanov[7], Gerard Drewes[5], Pablo Gamallo[4], Sonja Ghidelli-Disse[5], Stephanie Gresham[6], Elena Jiménez[4], Jaime de Mercado[4], Esther Pérez-Herrán[4], Esther Porras-De Francisco[4], Joaquín Rullas[4], Patricia Casado[4], Florence Leroux[1,8], Catherine Piveteau[1], Mehdi Kiass[9], Vanessa Mathys[9], Karine Soetaert[9], Véronique Megalizzi[10], Abdalkarim Tanina[10], René Wintjens[10], Rudy Antoine[2], Priscille Brodin[2,8], Vincent Delorme[2]‡, Martin Moune[2], Kamel Djaout[2], Stéphanie Slupek[2], Christian Kemmer[11], Marc Gitzinger[11], Lluis Ballell[4], Alfonso Mendoza-Losana[4]§, Sergio Lociuro[11]*, Benoit Deprez[1,8]*, David Barros-Aguirre[4], Modesto J. Remuiñán[4]*†, Nicolas Willand[1]*†, Alain R. Baulard[2,8]*†

The sensitivity of *Mycobacterium tuberculosis*, the pathogen that causes tuberculosis (TB), to antibiotic prodrugs is dependent on the efficacy of the activation process that transforms the prodrugs into their active antibacterial moieties. Various oxidases of *M. tuberculosis* have the potential to activate the prodrug ethionamide. Here, we used medicinal chemistry coupled with a phenotypic assay to select the N-acylated 4-phenylpiperidine compound series. The lead compound, SMARt751, interacted with the transcriptional regulator VirS of *M. tuberculosis*, which regulates the *mymA* operon encoding a monooxygenase that activates ethionamide. SMARt751 boosted the efficacy of ethionamide in vitro and in mouse models of acute and chronic TB. SMARt751 also restored full efficacy of ethionamide in mice infected with *M. tuberculosis* strains carrying mutations in the *ethA* gene, which cause ethionamide resistance in the clinic. SMARt751 was shown to be safe in tests conducted in vitro and in vivo. A model extrapolating animal pharmacokinetic and pharmacodynamic parameters to humans predicted that as little as 25 mg of SMARt751 daily would allow a fourfold reduction in the dose of ethionamide administered while retaining the same efficacy and reducing side effects.

INTRODUCTION

The DOTS (Directly Observed Treatment Short Course) strategy launched by the World Health Organization (WHO) in 1995, followed by the "End TB Strategy," has had a substantial impact on the treatment of tuberculosis (TB). Nonetheless, in its latest report, WHO estimates that, in 2020, 10 million individuals developed TB and 1.5 million people died, including 214,000 in the HIV-positive population (*1*). The impact of the coronavirus disease 2019 (COVID-19) pandemic has reversed years of global progress in reducing the number of people who die from TB, with the estimated number of deaths in 2020 the same as that in 2017. In addition, the increasing number of isolates of *Mycobacterium tuberculosis*, the pathogen that causes TB, that are resistant to the core antibiotics of the recommended anti-TB polytherapy is now putting the whole WHO strategy at risk and is a major obstacle to the objective of "a world free from TB" by 2035 (*2*). Worldwide in 2020, close to half a million people developed rifampicin-resistant TB, of which 78% had multidrug-resistant TB (MDR-TB) (*1*). The efficacy of the DOTS treatment is about 60% for MDR-TB and can drop to 26% for extensively drug-resistant TB (XDR-TB) (that is, MDR-TB with resistance to fluoroquinolones and one injectable aminoglycoside) (*3*). In this context, the End TB Strategy proposed by WHO includes the development of new universal treatments for TB based on pan-active drugs and the treatment of individuals with latent TB at high risk of TB reactivation. The recent discovery of antibiotics such as bedaquiline, delamanid, and pretomanid suggests the possibility of assembling completely new anti-TB drug regimens. Nevertheless, more drug candidates are needed to ensure that new efficacious and safe drug combinations can be developed.

[1]Univ. Lille, Inserm, Institut Pasteur de Lille, U1177 - Drugs and Molecules for living Systems, F-59000 Lille, France. [2]Univ. Lille, CNRS, Inserm, CHU Lille, Institut Pasteur de Lille, U1019 - UMR9017 - CIIL - Center for Infection and Immunity of Lille, F-59000 Lille, France. [3]BioVersys SAS, Lille, France. [4]GSK, Tres Cantos R&D, PTM, Tres Cantos, 28760 Madrid, Spain. [5]Cellzome GmbH . A GSK Company, 69117 Heidelberg, Germany. [6]GSK, David Jack Centre for R&D, Park Road, Ware, Hertfordshire SG12 ODP, UK. [7]GSK, Clinical Pharmacology and Experimental Medicine, 1250 South Collegeville Road, Collegeville, PA 19426, USA. [8]Univ. Lille, CNRS, Inserm, CHU Lille, Institut Pasteur de Lille, US 41 - UAR 2014 - PLBS, F-59000 Lille, France. [9]National Reference Center for Tuberculosis and Mycobacteria, Sciensano, Brussels, Belgium. [10]Microbiology, Bioorganic and Macromolecular Chemistry, Facult. de Pharmacie, Universit. Libre de Bruxelles, Brussels, Belgium. [11]BioVersys AG, Basel, Switzerland.
*Corresponding author. Email: alain.baulard@inserm.fr (A.R.B.); modesto.b.remuinan@gsk.com (M.J.R.); nicolas.willand@univ-lille.fr (N.W.); benoit.deprez@univ-lille.fr (B.D.); sergio.lociuro@bioversys.com (S.L.)
†These authors contributed equally to this work.
‡Present address: Tuberculosis Research Laboratory, Discovery Biology, Institut Pasteur Korea, Gyeonggi-do, Republic of Korea.
§Present address: Dept. Bioingeniería e Ingeniería Aeroespacial, Universidad Carlos III de Madrid, Madrid, Spain.

Many antibiotics against *M. tuberculosis* are prodrugs that need to be converted to active compounds by specific mycobacterial enzymes. This is the case for isoniazid, pyrazinamide, *p*-aminosalicylic acid, ethionamide (ETH), prothionamide, delamanid, pretomanid [reviewed in (*4*)], clofazimine (*5*), and TBA-354 (*6*). The Baeyer-Villiger monooxygenase EthA (Rv3854c) (*7*–*9*) catalyzes the activation of ETH in *M. tuberculosis*. This transformation leads to the formation of a stable covalent adduct between ETH and nicotinamide adenine dinucleotide (NAD), which inhibits the enoyl reductase InhA involved in mycolic acid biosynthesis (*10*, *11*). The production of EthA is regulated by the TetR-type transcriptional repressor EthR (Rv3855) (*12*). We and others have shown that small molecules specifically developed to inhibit EthR boost the production of EthA, which increases the activation and thus the antibacterial activity of ETH (*13*–*23*). More recently, we identified compounds activating an alternative activation pathway for ETH. SMARt420, the lead compound of this new chemical series, was shown to stimulate the expression of the putative oxidoreductase EthA2 (Rv0077c) by inhibiting the transcriptional repressor EthR2 (Rv0078). Consequently, SMARt420 was able to reverse resistance to ETH in *M. tuberculosis* strains carrying mutations in *ethA* (*24*).

Here, we set out to design dual inhibitors of EthR and EthR2 using the crystal structures of both proteins and then selected active compounds through phenotypic and functional assays. Unexpectedly, we identified small molecules controlling the expression of the *virS-mymA* regulon of *M. tuberculosis*, which was recently reported to be able to activate ETH (*25*). We show that the lead compound of this family of small molecules, SMARt751, was effective at boosting the efficacy of ETH against *M. tuberculosis* in vitro and in vivo as well as against a number of ETH-resistant *M. tuberculosis* clinical isolates.

RESULTS

Rational design and optimization of small molecules that boost ETH activity in vitro

Previously identified small molecules that boost ETH activity, BDM41906 and SMARt420, share common chemical features (Fig. 1A), with only residual binding to EthR by SMARt420 and no affinity for EthR2 for BDM41906 (*24*). With the objective of targeting both regulators with one unique small molecule, and on the basis of the structure-activity relationships in the two different chemical series, we hypothesized that an *N*-trifluorobutyrylpiperidine motif substituted on position 4 of the piperidine by a phenyl ring could accommodate the ligand-binding domain of both EthR and EthR2. Compound SMARt647 was designed (Fig. 1B) and synthesized according to these criteria (see Supplementary Materials and Methods).

Binding of SMARt647 to EthR and EthR2 was then assessed by determining the denaturation temperature of these two proteins in complex with this small molecule. SMARt647 increased the thermostability of EthR by 3.5°C and of EthR2 by 0.5°C (Table 1). To measure the ability of SMARt647 to block binding of EthR and EthR2 to their respective operator DNA, we used our previously described synthetic mammalian gene circuit with a secreted alkaline phosphatase readout (*24*). This assay showed that SMARt647 was less potent than BDM41906 and SMARt420 at blocking binding of the DNA to EthR and EthR2, respectively (Table 1, fig. S1, and data file S1). In contrast to these results, SMARt647 [half maximal effective concentration (EC_{50}) = 11 nM] was more potent than SMARt420 (EC_{50} = 1.5 μM) and BDM41906 (EC_{50} = 0.87 μM) at boosting by 10-fold the activity of ETH against *M. tuberculosis* in vitro.

In preparation for in vivo efficacy studies in mice, we first measured the metabolic stability of SMARt647 in liver microsomes. The microsomal study indicated that SMARt647 was rapidly metabolized to a less potent phenolic derivative with an intrinsic clearance of 23.6 ml min^{-1} g^{-1} liver. Formulated in hydroxypropyl-β-cyclodextrin, and given orally at a dose of 20 mg/kg of body weight to C57BL/6 female mice, SMARt647 showed a relatively poor systemic exposure [C_{max} = 40 ng/ml, area under the curve (AUC) = 25.7 ng·hour/ml] (Fig. 1, C and D). Liquid chromatography–tandem mass spectrometry (LC-MS/MS) analysis performed on blood samples from mice treated with SMARt647 revealed that the phase 1 phenolic metabolite was glucuronidated in vivo. Introduction of a fluorine atom at the metabolically unstable para-position of the phenyl ring of SMARt647 led to SMARt751 (see Fig. 1B and Supplementary Materials and Methods), which showed improved metabolic stability in mouse microsomes [intrinsic clearance (CL_{int}) = 0.74 ml min^{-1} g^{-1} liver] (Fig. 1D). The in vitro potency of SMARt751 was equivalent to that of SMARt647; a concentration of 10 nM SMARt751 was sufficient to boost the MIC_{50} of ETH half of the lowest

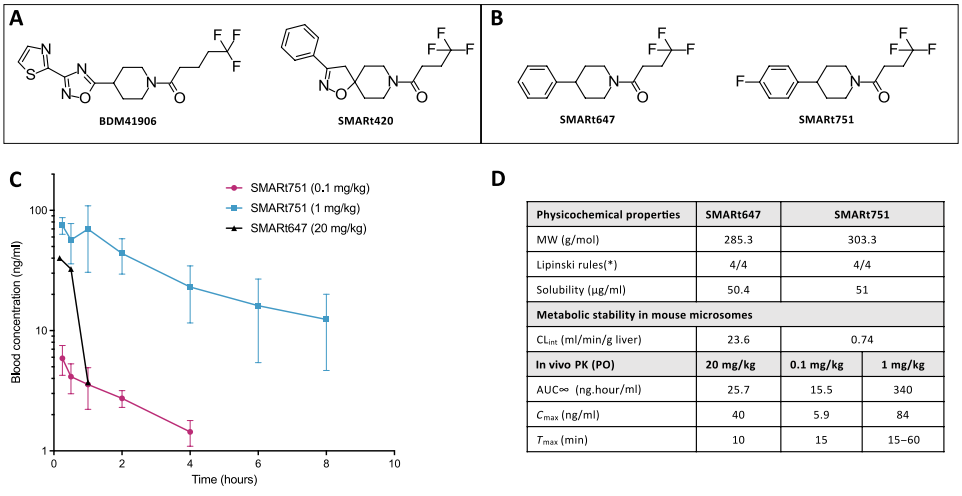

D

Physicochemical properties	SMARt647	SMARt751	
MW (g/mol)	285.3	303.3	
Lipinski rules(*)	4/4	4/4	
Solubility (μg/ml)	50.4	51	
Metabolic stability in mouse microsomes			
CL_{int} (ml/min/g liver)	23.6	0.74	
In vivo PK (PO)	**20 mg/kg**	**0.1 mg/kg**	**1 mg/kg**
AUC∞ (ng.hour/ml)	25.7	15.5	340
C_{max} (ng/ml)	40	5.9	84
T_{max} (min)	10	15	15–60

Fig. 1. Chemical structures of ethionamide potentiators and PK profiles of SMARt751 and SMARt647. (**A**) Chemical structures of the EthR inhibitor BDM41906 [5,5,5-trifluoro-1-[4-(3-thiazol-2-yl-1,2,4-oxadiazol-5-yl)-piperidin-1-yl]pentan-1-one] and the EthR2 inhibitor SMARt420 [4,4,4-trifluoro-1-(3-phenyl-1-oxa-2,8-diazaspiro[4.5]dec-2-en-8-yl)butan-1-one]. (**B**) Chemical structures of the two members of the N-acylated 4-phenylpiperidine series of VirS inhibitors: SMARt647 [4,4,4-trifluoro-1-(4-phenyl-1-piperidyl)butan-1-one] and the lead compound SMARt751 [4,4,4-trifluoro-1-[4-(4-fluorophenyl)-1-piperidyl]butan-1-one]. (**C**) Blood concentrations in mice over 10 hours after a single oral administration of SMARt751 [0.1 mg/kg (pink) or 1 mg/kg (blue)] or SMARt647 [20 mg/kg (black)] (n = 3 mice per group). Error bars indicate SD. SMARt751 was formulated in methylcellulose, and SMARt647 was formulated in hydroxypropyl-β-cyclodextrin. (**D**) Physicochemical properties, in vitro metabolic stability in mouse microsomes, and in vivo PK of SMARt647 and SMARt751 in mice. (*) Both compounds have less than 5 H-bond donors and 10 H-bond acceptors, a molecular weight (MW) smaller than 500 g/mol, and a calculated Log P (CLogP) smaller than 5, which corresponds to the best score (four of four) in the Lipinski rules aiming to predict absorption and permeation of orally administered compounds (*55*).

Table 1. The potency of ethionamide potentiators against *M. tuberculosis*. ΔTm-EthR and ΔTm-EthR2 values are the differences (in °C) between the melting temperature (measured by thermal shift assay) of the corresponding proteins alone and in combination with one of the listed compounds. BV-EthR and BV-EthR2 IC_{50} values are the concentration of the compound that displaces 50% of the binding of the corresponding protein to its DNA operator measured using a mammalian reporter gene circuit (SEAP) (fig. S1). ETH-Boost EC_{50} values are the concentration of compound required to make ETH 10 times more efficacious against either the *M. tuberculosis* H37Rv strain or *M. tuberculosis* ETH-resistant E1 strain (*ethA*$^-$).

Compound	ΔTm-EthR (°C)	ΔTm-EthR2 (°C)	BV-EthR (IC_{50}; μM)	BV-EthR2 (IC_{50}; μM)	ETH-Boost on *M. tuberculosis* (H37Rv) (EC_{50}; μM)	ETH-Boost on *M. tuberculosis ethA*$^-$ (E1 strain) (EC_{50}; μM)
BDM41906	8.49 ± 0.48	−0.25 ± 0.12	0.2	>10	0.874 ± 0.258	30 ± 9.394
SMARt420	1.57 ± 0.15	1.91 ± 0.25	3.1	0.2	1.518 ± 0.461	3 ± 0676
SMARt647	3.54 ± 0.27	0.42 ± 0.25	8.4	>10	0.011 ± 0.007	0.017 ± 0.010
SMARt751	3.45 ± 0.27	1.24 ± 0.10	–	–	0.012 ± 0.007	0.033 ± 0.007

concentration of ETH that inhibit the bacterial growth against the *M. tuberculosis* H37Rv strain by 10-fold (Table 1 and data file S1). Similarly, 33 nM SMARt751 was sufficient to reverse resistance to ETH in *M. tuberculosis* strain E1, which carries a mutation in EthA replacing Gly_{343} with Ala. The higher intrinsic metabolic stability of SMARt751 resulted in improved pharmacokinetics (PK) in mice (Fig. 1D). SMARt751 was rapidly absorbed after oral administration to C57BL/6 female mice at doses of 0.1 and 1 mg/kg of body weight. The maximum blood concentrations obtained at these two doses were 5.9 ng/ml (19.4 nM) and 84 ng/ml (278 nM), respectively. Administration of 1 mg/kg was sufficient to maintain a blood concentration above the in vitro EC_{50} (10 nM) for more than 8 hours.

A low dose of SMARt751 boosts ETH activity in mice

The ability of SMARt751 to boost ETH activity in vivo was first evaluated in a fast-acute mouse model of TB (*26*). Mice infected with *M. tuberculosis* strain H37Rv were given different dose combinations of SMARt751 and ETH for 8 days. An ETH dose response curve was performed in the absence or presence of different doses of SMARt751 (Fig. 2). The efficacy of the various combinations was compared using their respective ED99 values, that is, the efficacious dose eliminating at least 99% of the bacteria in the lungs (upper dashed line in Fig. 2). ED99 and 95% confidence interval (95% CI) were calculated for each experimental condition. ED99 shifted from 23 mg/kg (95% CI, 18 to 31 mg/kg) when ETH was used alone to <3 mg/kg for ETH used in combination with SMARt751 (0.1 mg/kg). In contrast, SMARt751 given alone showed no effect on the bacterial pulmonary load in mice treated with doses ranging from 0.001 to 1 mg/kg of body weight (fig. S2). The treatment with SMARt751 (0.1 mg/kg) was sufficient for maximum boosting of ETH's activity because this concentration was as effective as the highest dose used in this assay (10 mg/kg) (Fig. 2). Although expected fluctuations from one mouse experiment to another were observed, ETH ED99 shifts were systematically obtained in three additional experiments using SMARt751 (either 0.1 or 10 mg/kg) (fig. S3).

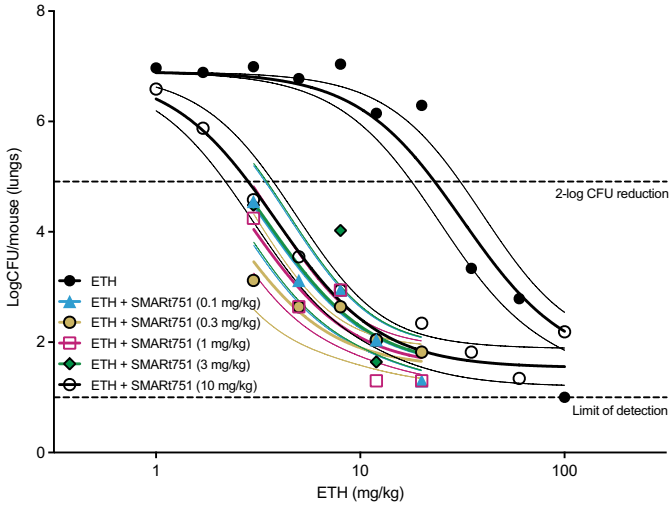

Fig. 2. Lung bacterial load in mice after 8 days of treatment. Mice were infected with 10^5 CFU of *M. tuberculosis* H37Rv by intratracheal instillation. Treatment (ETH or ETH + SMARt751) was started the next day (acute model of TB) and given once daily for 8 days. Lung CFUs were counted on day 9, 24 hours after the last administration. Each point represents data from an individual mouse that received ETH or ETH plus different doses of SMARt751. To serve as a reference, a full dose-response curve was established for ETH concentrations of 1 to 100 mg/kg mouse body weight (black circles). In this acute TB mouse model, the dose of ETH eliminating at least 99% of the bacteria in the lungs, that is, 2-log reduction of CFU or ED99, was 23 mg/kg (95% CI, 18 to 31 mg/kg). ETH was given with different concentrations of SMARt751 ranging from 0.1 to 10 mg/kg. The pulmonary bacterial load was assessed by enumeration of bacterial CFU in lung homogenates spread on agar plates. LogDose versus logCFU were fitted to a four-parameter sigmoidal curve where the top plateau (mean CFU value in untreated mouse lungs) and the bottom plateau (mean CFU value in high-dose ETH control groups determined in previous experiments) were constrained. Dashed horizontal lines show 95% CI for each curve. The estimated ED99 of ETH administered in combination with SMARt751 was calculated from the 95% CI of ED99 for ETH monotherapy (see fig. S3). This experiment is representative of four independent experiments (fig. S3).

SMARt751 has a long-lasting boosting effect on ETH activity in vitro and in vivo

To evaluate whether continuous contact of *M. tuberculosis* with SMARt751 was required to boost ETH activity, fluorescent bacteria were treated for 24 hours with 1 μM SMARt751, and then were washed and analyzed by a phenotypic assay. Figure 3A shows that bacteria pretreated with SMARt751 and subsequently washed were as sensitive to ETH as bacteria continuously exposed to the combination of ETH and SMARt751. This pretreatment and long-lasting effect of SMARt751 was tested in a fast-acute mouse model of TB, where infected mice were treated for 8 days with ETH (10 mg/kg daily) combined with one, two, four, or eight doses of SMARt751 (1 mg/kg per dose). Administration of SMARt751 every 2 or 4 days

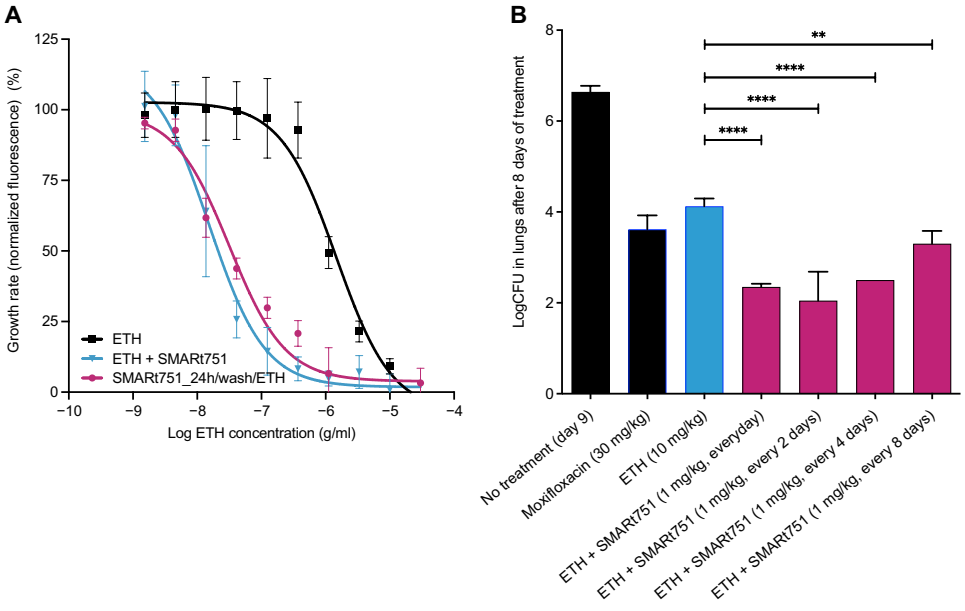

Fig. 3. Long-lasting effect of SMARt751 on ETH activity in vitro and in vivo. (**A**) Dose-response growth curve for the *M. tuberculosis* H37Rv strain labeled with GFP. Bacteria were treated with 1 μM SMARt751 for 24 hours and then were washed and treated with various doses of ETH for 5 days (pink curve). The dose-response growth curve for bacteria treated with ETH alone (black curve) or ETH in combination with 1 μM SMARt751 (blue curve) is shown. Each point on each curve is the average of two independent experiments, each with three biological replicates (data file S1). (**B**) Efficacy (reduction in lung CFU) of daily doses of ETH alone (10 mg/kg of body weight; blue) or combined with SMARt751 (1 mg/kg of body weight; pink) in infected mice. Doses were administered every 2, 4, or 8 days. Control infected mice received moxifloxacin daily at 30 mg/kg of body weight. $^{**}P \leq 0.01$; $^{****}P \leq 0.0001$ [one-way analysis of variance (ANOVA) with Dunnett's multiple comparisons test]. This experiment included a minimum of two mice per data point (fig. S4).

together with daily doses of ETH was as efficient at boosting ETH activity as daily coadministration (Fig. 3B and fig. S4).

SMARt751 efficiently boosts ETH activity in mice with chronic TB

The potency of SMARt751 was then measured in a chronic mouse model of TB. C57BL/6 mice were infected with ~100 colony-forming units (CFU) of *M. tuberculosis H37Rv*; bacilli reached a steady-state infection of ~10^6 bacteria per lung 6 weeks later. Combinations of ETH and SMARt751 were then given orally daily for 8 weeks. SMARt751 (0.3 mg/kg) was sufficient to shift the ED99 dose of ETH from 24 mg/kg (95% CI, 19 to 31) to 9.2 mg/kg (95% CI, 7 to 12) (Fig. 4). Comparable ETH ED99 shifts were obtained in two additional experiments using SMARt751 (10 mg/kg) (fig. S5). The maximum effect of the dose response (low plateau) observed with ETH alone was the same as that obtained in the presence of SMARt751, showing that SMARt751 has no intrinsic antibacterial activity (Fig. 4).

To quantify the boosting effect of SMARt751 on ETH activity at the various doses of ETH tested in mice, we analyzed the efficacy of ETH as a function of blood concentration rather than dose. Pre- or coadministration of SMARt751 with ETH to mice had no influence on the PK profile of ETH (Fig. 5A and fig. S6), confirming that the observed increase in ETH potency in vivo was mediated by SMARt751 and not by PK drug-drug interactions. Then, we determined whether the exposure of ETH was linear for doses ranging from 3.4 to 90 mg/kg. Oral administration of ETH to mice revealed nonlinear PK (Fig. 5B), in contrast to what has been described in humans (*27*, *28*). Considering the relationship between dose and total systemic exposure to drug (AUC = Dose × *F*/CL, where *F* is the oral bioavailability and CL is the blood clearance), the boosting effect of SMARt751 on ETH activity in mice was derived from the ratio $AUC_{ED99}/AUC^{B}_{ED99}$. AUC_{ED99} and AUC^{B}_{ED99} are the total systemic exposures to ETH required to obtain 99% reduction in bacterial load in mouse lung in the absence (AUC_{ED99}) or presence (AUC^{B}_{ED99}) of SMARt751, respectively. We calculated that ETH activity was boosted about 19-fold in the fast-acute mouse model of TB (640 ng·hour/ml versus 34 ng·hour/ml) and 6-fold in the chronic mouse model of TB (640 ng·hour/ml versus 105 ng·hour/ml) (table S1).

SMARt751 reverses resistance to ETH in mice infected with *M. tuberculosis* strain E1

Next, we examined the combination of ETH and SMARt751 in mice infected with *M. tuberculosis* strain E1 that is resistant to ETH. C57BL/6 mice were infected by intratracheal instillation with ~10^5 CFU of *M. tuberculosis* strain E1. Seven days after infection, the mice were treated with ETH alone or in combination with SMARt751 at 6 mg/kg body weight. Daily administration by gavage of up to 50 mg/kg of ETH alone for 21 days was ineffective at reducing the bacterial load in mouse lungs, confirming the resistance of *M. tuberculosis* strain E1 to ETH (Fig. 6). In contrast, treatment with a combination of ETH (25 mg/kg body weight) and SMARt751 (6 mg/kg body weight) resulted in a substantial ~6.3-log reduction in lung CFU for this mouse group, showing the strong bactericidal activity of the drug combination against this ETH-resistant *M. tuberculosis* strain (Fig. 6 and fig. S7). The efficacy of the combination of ETH and SMARt751 was better than the efficacy observed with 25 mg/kg of the frontline TB drug isoniazid. No detectable effect was observed with SMARt751 administered alone, confirming that the activity of the drug combination against *M. tuberculosis* strain E1 was specifically due to the reversal of the resistance to ETH.

SMARt751 reverses ETH resistance in *M. tuberculosis* clinical isolates

M. tuberculosis mechanisms of resistance to ETH are diverse, possibly including mutations in *ethA*, *ethR*, *inhA*, or *mshA* (*29*). The ability of SMARt751 to reverse ETH resistance was assessed using a panel of 37 *M. tuberculosis* clinical isolates (from seven different lineages) resistant to ETH (with a MIC of ETH ≥ 4 μg/ml). All of the 32 TB-MDR clones were also resistant to isoniazid including 10 that were pre-XDR and 3 that were XDR. Ten isolates were mutated in *ethA*, and 12 were mutated in the *inhA* promoter (table S2).

Standardized respirometry experiments in vitro (MGIT960) showed that for 33 of the 37 ETH-resistant *M. tuberculosis* isolates, 150 nM SMARt751 was sufficient to reverse the MIC of ETH to ≤0.8 μg/ml.

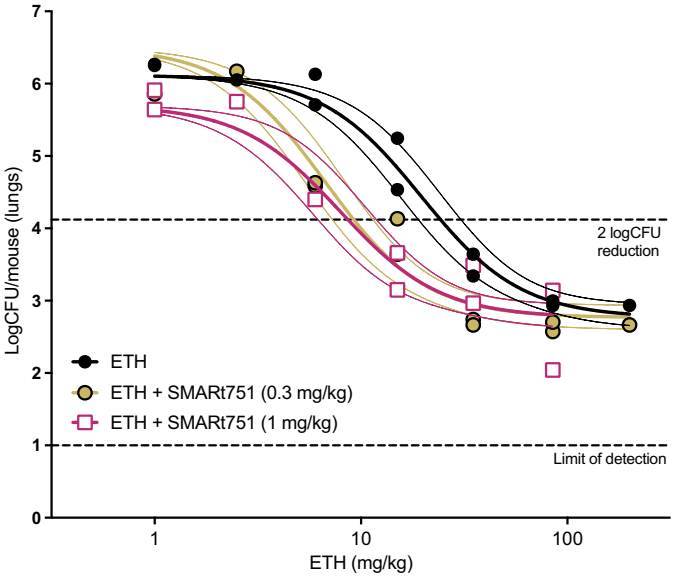

Fig. 4. Lung bacterial load in mice after 2 months of treatment. Dose-response curves comparing ETH alone (black circles) and ETH in combination with SMARt751 at doses of 0.3 mg/kg (yellow) or 1 mg/kg (pink) in mice chronically infected with *M. tuberculosis* are shown. After 2 months of oral treatment once daily, the pulmonary bacterial load was assessed by enumeration of bacterial CFU in lung homogenates spread on agar plates. Two mice were used per time point and drug combination. The intersection points between the dashed line and the curves indicate the dose of ETH that eliminates 99% of the bacterial load in mouse lungs (ED99). ED99 was 24 mg/kg in the absence of SMARt751 (black curve) and 9.2 mg/kg in the presence of SMARt751 (pink curve). Data were fitted to a four-parameter sigmoidal response curve. The top of the curve was constrained to the average CFU of untreated mice (for the black curve) or mice treated with SMARt751 at 0.3 mg/kg (for the yellow curve) or 1 mg/kg (for the pink curve). The bottom of all curves was constrained to a shared value estimated for all the curves together. Dashed horizontal lines show 95% CI for each curve. Curves are representative of three independent experiments performed at different doses (fig. S5).

Of these 33 isolates, 14 were randomly selected and, for all of them, 10 nM SMARt751 was sufficient to reduce the MIC of ETH to <0.8 μg/ml (table S2). One of the 37 clinical isolates was highly resistant to ETH (≥256 μg/ml) and required 300 nM SMARt751 to shift the MIC of ETH to 0.8 μg/ml. The 3 remaining isolates of the 37 ETH-resistant clinical isolates showed a MIC of ETH of 2 μg/ml in the presence of 300 nM SMARt751. The genomes of these three clinical isolates were fully sequenced. Whereas the three genome sequences confirmed mutations in the *inhA* promoter and revealed common nucleotide polymorphisms seen in the other clinical isolates, no single-nucleotide polymorphisms (SNPs) in genes specifically involved neither in ETH resistance nor in the *mymA* operon were identified. Thus, SMARt751 reversed resistance to ETH in all clinical isolates tested, independently of their lineage or resistance to other antibiotics including isoniazid.

PK of SMARt751 in preclinical species

Physicochemical properties, in vitro ADME (absorption, distribution, metabolism, and excretion), and in vivo drug metabolism and PK profiles of SMARt751 were evaluated in preclinical species (mouse, rat, and dog) to support further development of SMARt751 and dose prediction modeling in humans. SMARt751 displayed satisfactory solubility (53 to 103 μg/ml) in physiologically relevant media. Permeability values across Madin-Darby canine kidney cell monolayers in vitro were high in both directions with no notable efflux (table S3). Therefore, neither solubility nor permeability was expected to limit oral absorption of SMARt751. The intrinsic clearance (CL_{int}) of SMARt751 was below the lower limit of quantification (LLOQ) in assays using human liver microsomes or human hepatocytes. Moderate plasma protein binding and low blood-to-plasma partitioning ratios were observed in preclinical species and in human blood (table S3).

The PK of SMARt751 after intravenous or oral administration at various doses was evaluated in rodents and dogs. The compound exhibited moderate to high in vivo clearance (that had been predicted given the intrinsic clearance in hepatocytes) and a moderate to high volume of distribution (table S4). Oral bioavailability was low in rats and moderate in mice and dogs, in agreement with an expected first-pass effect. Human PK parameters were estimated using a physiologically based PK model. This model accurately predicted (with only a twofold error) the experimentally observed PK profiles in preclinical species based on the corresponding in vitro ADME characteristics. The prediction of PK for SMARt751 in human estimated a moderate clearance (9 ml min^{-1} kg^{-1}), a high volume of distribution (7.8 l/kg), and a moderate oral bioavailability (50%).

Exposure at the target site of action over a desired period of time is fundamental to elicit the desired effect for any treatment. In our study, the desired effect required exposure to both ETH and SMARt751. ETH shows high permeability, solubility, and volume distribution, which allows it to cross the blood-brain barrier and to achieve concentrations in the brain and cerebrospinal fluid equivalent to those in plasma. Similarly, SMARt751 displays high passive permeability and oral bioavailability. SMARt751 is not an in vitro substrate of P-glycoprotein (P-gp) given that the efflux ratio measured was similar in the absence and presence of P-gp inhibitors (see Supplementary Materials and Methods). The in vitro permeability of SMARt751 translated into a high brain partition coefficient (Kp) in mice, with an estimated brain/blood ratio of 1.7:1.8 (fig. S8A). These values remained unchanged after pretreatment with the P-gp inhibitor elacridar (fig. S8B) (*30*). These data support a perfusion-limited, physiologically based PK model for SMARt751 distribution in vivo, suggesting that organs may be similarly exposed to ETH and SMARt751. Nevertheless, in vitro and in vivo data showed a long-lasting boosting effect of SMARt751 on ETH activity (Fig. 3), suggesting that the active concentrations of the two drugs may not need to be reached in a synchronized manner.

Modeling ETH activity when combined with SMARt751 in human

Using the efficacy data from the acute and chronic TB mouse models together with the PK of ETH and ADME properties of SMARt751, we estimated a set of pharmacodynamic (PD) parameters in mice (*31*). The translation and scaling of these parameters from mouse to human assumed (*1*) that the growth rates and maximum killing rates for *M. tuberculosis* exposed to ETH and SMARt751 were the same in both mouse and human and (*2*) that the unbound drug concentration in plasma was the driver of both ETH and SMARt751 efficacy. Considering the scaled PD and PK parameter distributions of ETH in a human adult cohort (*27*), the early bactericidal activity in the first 14 days of treatment (EBA_{0-14}) was simulated to investigate the effect of SMARt751 on three different daily doses of ETH (250, 500, and 750 mg) (Fig. 7). The simulations indicated that as little as 25 mg of SMARt751 daily (0.35 ± 0.1 mg/kg body weight) would drive a fourfold reduction in any of the three ETH doses while keeping the

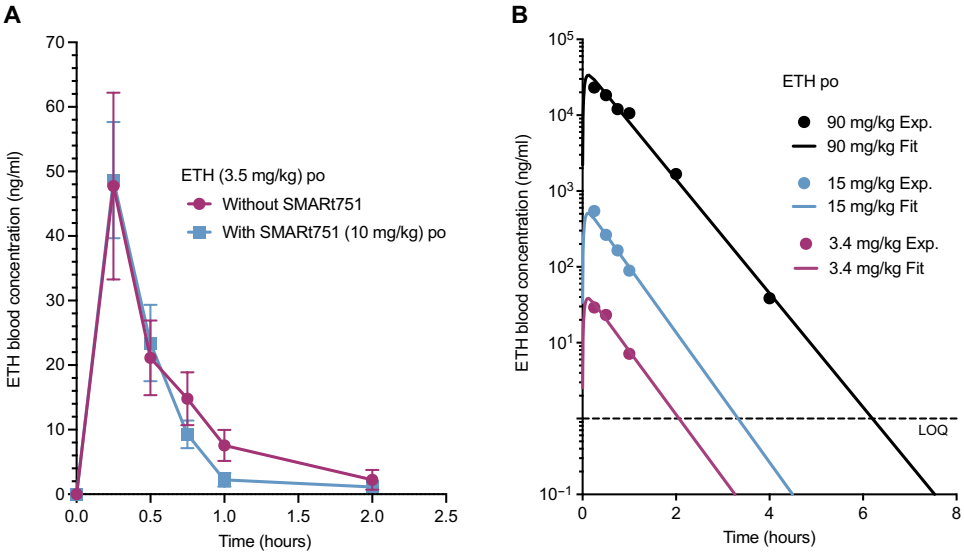

Fig. 5. Blood concentration–time curves after a single oral administration of ETH. (**A**) Whole blood concentration–time curves after a single oral administration (per os, by mouth) of ETH (3.5 mg/kg of body weight) to mice either without (pink) or with (blue) coadministration of SMARt751 (10 mg/kg) (three mice per group). (**B**) Experimental whole blood concentration–time values (Exp.) after a single oral administration to mice of ETH at doses of 3.4 mg/kg (pink), 15 mg/kg (blue), or 90 mg/kg (black) of body weight (three mice per group). Estimated AUC from the three fitted curves (Fit) revealed the nonlinearity of ETH PK. The dashed line is the limit of quantification of ETH.

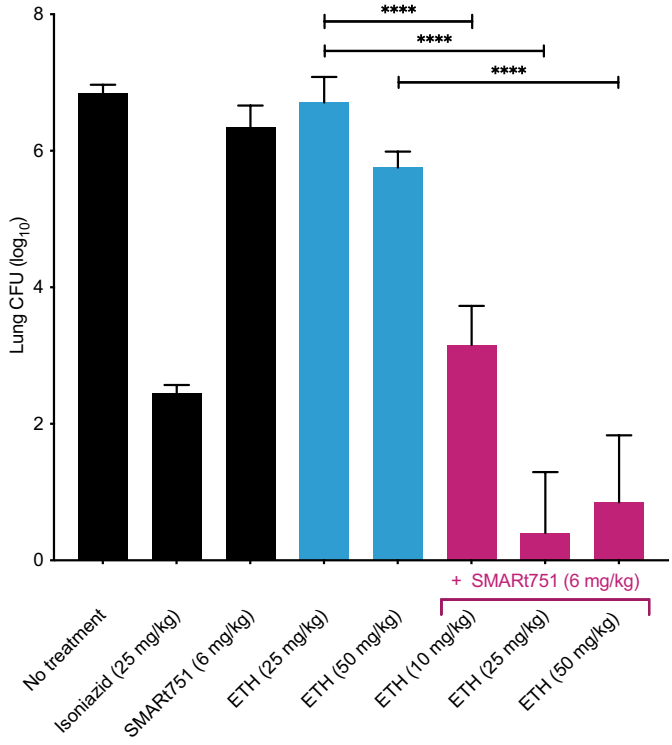

Fig. 6. ETH-SMARt751 efficacy in mice infected with ETH-resistant *M. tuberculosis*. The average log CFU per mouse lung after spreading lung homogenates from mice infected with ETH-resistant *M. tuberculosis* E1 strain on agar plates is shown (fig. S7). Mice ($n = 5$) infected with the ETH-resistant E1 strain were treated with ETH alone (blue) or with ETH plus different concentrations of SMARt751 (pink). Isoniazid was used at 25 mg/kg of body weight as a positive control. Treatment concentrations (mg/kg of body weight) are indicated. Data are means ± SD. ****$P \leq 0.001$, one-way ANOVA with Bonferroni's test.

same respective EBA_{0-14} performance (fig. S9). In particular, administration of 25 mg of SMARt751 daily was calculated to allow a reduction in the standard 750-mg daily dose of ETH to 188 mg.

Drug-drug interactions and safety of SMARt751

Taking into account that SMARt751 would have to be administered not only with ETH but also in combination with other antitubercular compounds, drug-drug interaction liabilities were evaluated. The potential of SMARt751 to directly inhibit cytochrome P450 (CYP) isoforms CYP1A2, CYP2C9, CYP2C19, CYP2D6, and CYP3A4 was evaluated in human liver microsomes with specific probe substrates. No inhibition by SMARt751was observed at concentrations of up to 25 μM for all isoforms tested, with the exception of CYP2C19 (IC_{50} = 2.1 μM). Complementary studies on CYP3A4 and CYP2C19 ruled out any time- or metabolism-dependent inhibition by SMARt751. The potential of CYP induction by SMARt751 was investigated in cultured human hepatocytes. The increase in expression of CYP1A2, CYP2D6, and CYP3A4 mRNA was less than twofold for concentrations of SMARt751 up to 10 μM (fig. S10). Considering the predicted blood concentrations of SMARt751 in humans (C_{max} = 23.5 ng/ml; 0.08 μM) and based on static models, our results suggest a low risk of SMARt751 perpetrating drug interactions or perturbing the PK of coadministered drugs.

In vitro safety pharmacology studies identified hERG (human ether-a-go-go-related gene) inhibition by SMARt751 with an IC_{50} of 27 μM. This potential effect of SMARt751 on QT interval prolongation and proarrhythmias was further assessed in the rabbit left ventricular wedge (RVW) model. QT interval shortening was observed (but not prolongation) at concentrations ranging from 10 to 100 μM with a maximum of 38%. A decrease in Tp-e interval was also observed at 100 μM. On the basis of previous in vitro safety pharmacology studies, the risk of arrhythmia in humans due to SMARt751 was considered low at the expected therapeutic dosage (*32*). The potential off-target pharmacological activity of SMARt751 was assessed in an enhanced cross-screen profiling panel of molecular and phenotypic assays involving targets such as ion channels, transporters, enzymes, and receptors (table S5). No activity higher than 50% (XC50) was detected with up to 1 μM SMARt751. Whereas evaluation identified some activity in two specific assays for γ-aminobutyric acid type A ($GABA_A$) antagonism and pregnane X receptor (PXR), follow-up studies concluded a low risk of secondary effects at the expected therapeutic dosage of SMARt751 for these two targets (fig. S10).

Last, preliminary toxicity studies of SMARt751 were carried out in mice using an oral repeat-dose protocol. Neither acute toxicity nor noticeable findings were observed after 4 days at a SMARt751 dose of 20 mg/kg per day, which corresponds to 60 times the observed therapeutic dose in mice. The findings observed at higher doses of SMARt751 at 60 and 200 mg/kg per day in the liver are described in fig. S10.

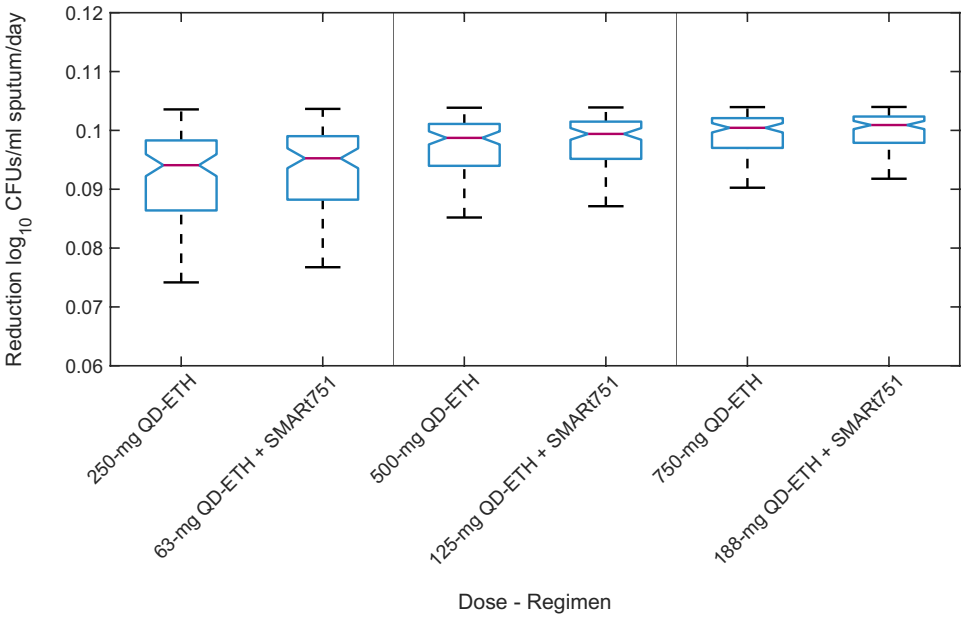

Fig. 7. Predicted effect of ETH-SMARt751 on reducing *M. tuberculosis* load in human lung. Simulations of the potential daily reduction (log_{10}) of bacterial CFUs in human lung after treatment with three ETH-SMARt751 combinations are shown. Simulations were based on a mathematical model that translated PK/PD parameters from mouse models to human (fig. S9). The drug-related parameters in mice were estimated from the measured CFUs in the acute and chronic in vivo experiments shown in Figs. 2 and 4. The PK of ETH in human was taken from (*27*). The daily reduction in bacterial load in human lungs over 14 days of treatment once a day (QD), also called early bactericidal activity, is a primary efficacy outcome in phase 2a trials testing TB drug regimens. The three pairs of comparisons show an estimated daily reduction (log_{10}) of bacterial CFUs in human lungs after treatment with three different doses of ETH alone (250, 500, and 750 mg) or ETH in combination with SMARt751 (63 mg ETH + 25 mg SMARt751; 125 mg ETH + 25 mg SMARt751; 188 mg ETH + 25 mg SMARt751). Each "box and whisker" plot shows the distribution of data obtained with the simulation. The box corresponds to the interquartile range of the estimated reduction with its median (pink), and lower and upper quartiles (blue). The minimum and maximum values of the dataset are indicated by the whiskers (black). The "notches" in the boxes represent the estimated 95% CI of the median. These simulations were performed with the function sbiosimulate using the software Simbiology/MATLAB (www.onlinemathlearning.com/box-plot.html) (fig. S9).

SMARt751 boosts ETH activation by controlling the *mymA* operon

Selection of spontaneous resistance mutants is an effective way to gain insight into the mode of action of small molecules and may help to develop molecular tools to monitor resistance during clinical trials and later clinical use. The minimal ETH concentration that allowed for the selection of ETH-resistant *M. tuberculosis* mutants in the absence of SMARt751 was 10 μg/ml (around fivefold the MIC). At this ETH concentration, spontaneous mutants appeared at a frequency of 4×10^{-8}. No mutant could be obtained by plating 10^8 bacteria on solid medium containing as low as 2 μg/ml of ETH in combination with 0.15 μM SMARt751. Combinations of ETH (0.5 μg/ml) and SMARt751 at 0.64, 0.32, and 0.15 μM were allowed for the selection of mutants at a frequency of 6×10^{-8}, 4×10^{-7}, and 3×10^{-6}, respectively.

Nine ETH-resistant *M. tuberculosis* mutants were selected for whole-genome sequencing. A relatively complex pattern of mutations was observed in these clones. All mutants harbored mutations in at least one gene of the regulon *virS-mymA* (table S6). Mutations in *ethA* were also observed in eight of the nine clones. In addition to their mutation in *ethA*, four of the eight clones had nonsynonymous SNPs in *Rv3083* (*mymA*), one had an SNP in *Rv3082c* (*virS*), and three had a 3.3-kb deletion covering the end of *rv3080* (*pknK*), *rv3081*, *virS*, and the beginning of *mymA*. MymA is a close homolog of the Baeyer-Villiger monooxygenase EthA and has recently been shown to activate thioamides (*25*). Loss of MymA function has been shown to confer some resistance to ETH, adding to the resistance associated with EthA loss of function (*25*). To rule out the involvement of other mutations identified in the nine spontaneous mutants, we tested the phenotype of *mymA*, *virS*, and *ethA* mutant *M. tuberculosis* strains (*25*). The first clone (Rv3083::TN), which contained a transposon in *mymA*, confirmed the inability of SMARt751 to boost ETH in this context (table S6). An equivalent phenotype was observed for clone 3-RM4, which contained a frameshift mutation in the region coding for the C-terminal portion of VirS (table S6). Last, the third clone (Rv3854c::TN) containing a transposon in *ethA* was shown to be resistant to ETH but sensitive to the SMARt751-ETH combination (table S6). These data show that resistance to the SMARt751-ETH combination can arise either from simultaneous mutations in *ethA* and the *mymA* regulon or more rarely by single mutations in the *mymA* regulon. In particular, the clone with a *virS* mutation (3-RM4) suggested that SMARt751 could control the expression of *mymA* by interacting with VirS (*33*).

To elucidate the mechanism of action of SMARt751, we analyzed the transcriptomic profile of *M. tuberculosis* exposed to 10 μM of this compound for 24 hours. Bacteria treated with SMARt751 showed 12 genes up-regulated more than threefold (Fig. 8A). The most overexpressed mRNAs corresponded to the *mymA* operon (*rv3083* to *rv3089*). No modification of *ethA* and *ethR* transcription was detected, which was supported by the modest thermostabilization of EthR by SMARt751 seen in a thermal shift assay (3.5°C instead of 8.5°C by the EthR-specific inhibitor BDM41906) (Table 1) (*13*). *rv0077c*, the gene corresponding to the oxidoreductase EthA2, was also overexpressed in the presence of SMARt751, highlighting the complex mechanisms involved in ETH activation (*24*).

Next, we quantified modifications of the *M. tuberculosis* global proteome upon treatment with SMARt751. Total protein extracts of two independent cultures of *M. tuberculosis* treated with 1 μM SMARt751 or with dimethyl sulfoxide (DMSO) for 72 hours were quantified by isobaric labeling–based mass spectroscopy. About 2200 proteins were identified. Treatment of the bacteria with SMARt751 led to the modification of the production of about 19 proteins (Fig. 8B). All of the proteins of the *mymA-virS* regulon were overexpressed upon treatment of the bacteria with SMARt751, in agreement with the transcriptomic experiments (Fig. 8A). The production of EthA and EthR was

A

Gene name	Identifier	Protein description	mRNA LFC upon SMARt751 treatment (*)	Protein LFC upon SMARt751 treatment (**)
mymA	*rv3083*	FAD-containing monooxygenase	73.28	22.31
sadH	*rv3085*	Putative oxidoreductase	68.98	13.89
lipR	*rv3084*	Putative acetyl-hydrolase	65.40	10.13
ethA2	*rv0077c*	Probable oxidoreductase	49.83	2.02
adhD	*rv3086*	Putative alcohol dehydrogenase D	29.03	9.57
rv0076	*rv0076c*	Probable membrane protein	23.00	n.i.
rv3087	*rv3087*	Putative diacylglycerol *O*-acyltransferase	17.40	12.90
tgs4	*rv3088*	Probable diacylglycerol *O*-acyltransferase	15.30	9.93
fadD13	*rv3089*	Long-chain fatty acid–CoA ligase	12.95	12.45
virS	*rv3082c*	HTH-type transcriptional regulator	5.23	28.18
rv3192	*rv3192*	Hypothetical ala and pro-rich protein	3.82	n.i.
rv0078	*rv0078*	Transcriptional regulator	3.07	1.06
deoR	*rv3066*	Probable transcriptional regulator	1.01	5.00
ethR	*rv3855*	HTH-type transcriptional regulator	1.15	0.43
ethA	*rv3854c*	FAD-containing monooxygenase	1.22	0.18

(*) Average of 3 biological replicates
(**) Average of 2 biological replicates
See table S5 for statistics
n.i. : not identified
LFC: linear fold change

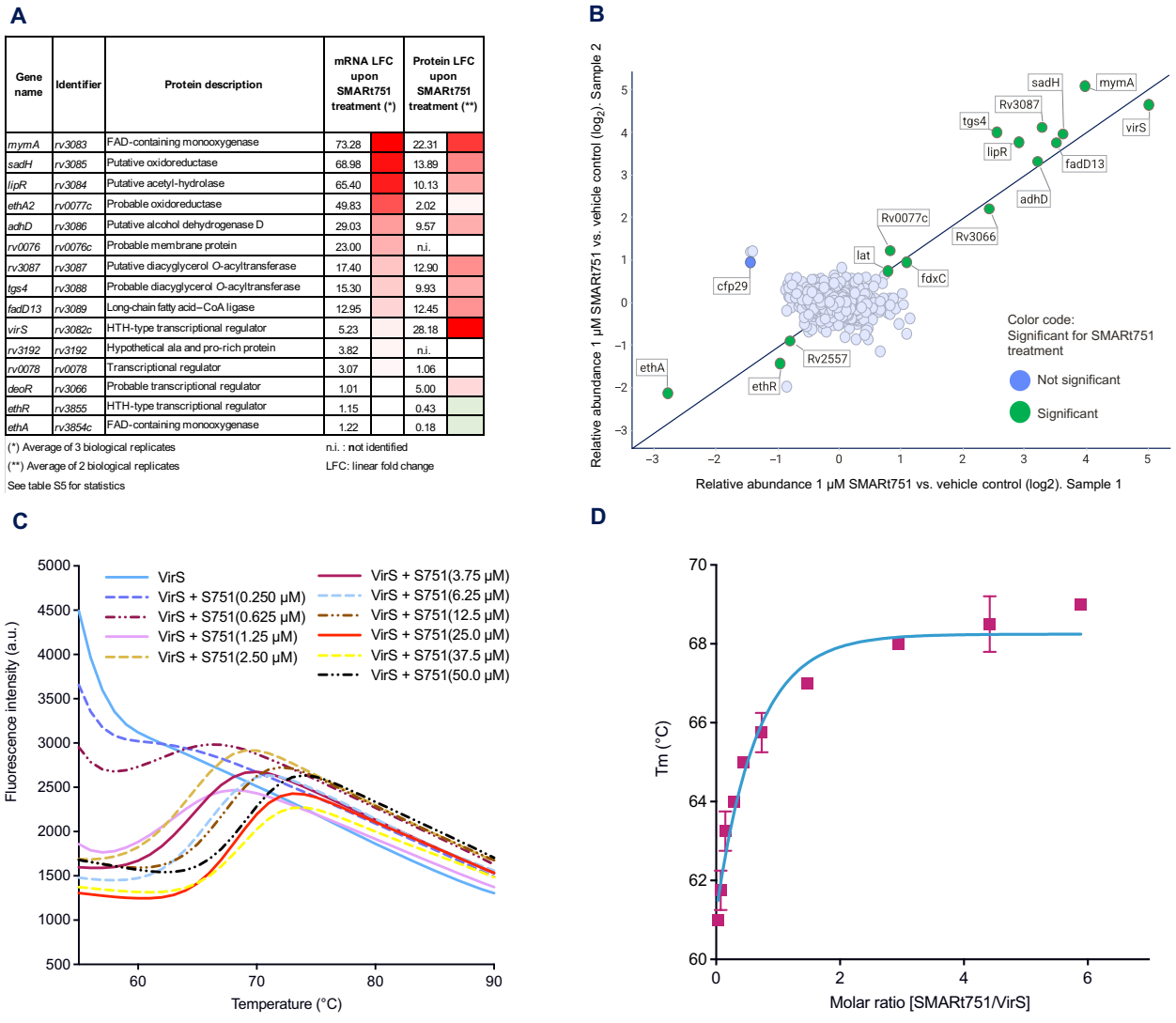

Fig. 8. Effect of SMARt751 on the transcriptome and proteome of *M. tuberculosis* and its interaction with VirS. (**A**) Comparison of the transcriptomic and proteomic profiles of the *M. tuberculosis* H37Rv strain treated with SMARt751. Transcriptomes were obtained from three independent cultures of *M. tuberculosis* H37Rv treated with 10 μM SMARt751 or DMSO as a control for 24 hours. Raw RNA-seq reads were processed with Illumina quality control tools using default settings, and analysis of RNA-seq data was conducted using the SPARTA open-source software package with default parameters (https://sparta.readthedocs.io/en/latest/) (data file S1). Proteomes were obtained from two independent experiments. For both experiments, values are the relative quantification of a total protein extract of *M. tuberculosis* H37Rv treated with 1 μM SMARt751 or with DMSO as a control for 72 hours. Protein quantification was done by isobaric labeling–based mass spectroscopy. Quantified proteins were required to contain at least two unique peptide matches. False discovery rate was <0.1%. The table reports genes for which we observed increased or decreased transcription of more than threefold and protein expression of more than twofold. (**B**) Comparison plot of the two independent proteomic experiments reported in (A) (sample 1 is on the *x* axis and sample 2 is on the *y* axis) that measures the abundance of proteins (boxes) after treatment of *M. tuberculosis* H37Rv cultures with SMARt751. Proteins for which expression in samples 1 and 2 was increased by a minimum of twofold upon SMARt751 treatment were considered relevant. (**C**) The binding of ligands can modify the thermal stability of a protein. Thermal denaturation of VirS (8.5 μM) was monitored using SYPRO Orange in the presence of SMARt751. Fluorescence signal was plotted as a function of temperature to get a sigmoidal melting curve for VirS. The presence of increasing SMARt751 concentrations (from 0.25 to 50 μM) led to a rightward shift in the inflection point of the curve, which corresponds to the melting temperature (Tm) of VirS. The Tm of VirS in the presence of the various concentrations of SMARt751 was calculated using the first derivative of fluorescence as a function of temperature ($-dF/dT$). (**D**) The plot shows the Tm of VirS as a function of the molar ratio of SMARt751 to VirS.

diminished under these conditions, although there was no regulation of these genes at the transcriptional level by SMARt751.

VirS mutants emerged by selecting clones spontaneously resistant to the ETH-SMARt751 combination. VirS (Rv3082c) is a major regulator of the *mymA* operon (*33*, *34*). To study the possible interaction between SMARt751 and VirS, we first adapted our synthetic mammalian reporter system. In this assay, binding of VirS to a chimeric DNA (including the intergenic region of the *virS-mymA* operon fused to the *hCMVmin* promoter) was predicted to drive expression of the downstream *SEAP* reporter gene. In the absence of SMARt751, we observed production of SEAP. Addition of SMARt751 led to strong inhibition of SEAP production. Together, these data show that SMARt751

modulated the ability of VirS to bind the promotor of the *mymA* operon (fig. S11). The thermostability of purified VirS was measured in the absence and presence of SMARt751. Thermal shift assays showed a dose-dependent thermostabilizing effect of SMARt751 on VirS of up to 8°C (Fig. 8C). Full stabilization of VirS was achieved in the presence of about two molar equivalents of SMARt751 (Fig. 8D).

DISCUSSION

There are some limitations to our study. Our demonstration of efficacy of the ETH-SMARt751 combination against *M. tuberculosis* clinical isolates was not exhaustive and was limited to ETH-resistant isolates that were available in the Sciensano collection. We also only demonstrated efficacy in murine models of infection. Animal allocations were not blinded to study scientists, and our mouse experiments were not randomized control preclinical studies; thus, we cannot exclude the possibility of selection bias. Modeling the efficacy of the ETH-SMARt751 combination was based on estimation and translation of parameters from mice to humans, assuming that bacterial growth rates and maximum killing rates were the same in both species, and that the unbound drug concentrations in plasma were the drivers of both ETH and SMARt751 efficacy. The clinical potential of SMARt751 cannot be fully established until safety and efficacy clinical trials are undertaken in humans. Although the mechanism of activation of ETH by SMARt751 involves the *virS-mymA* regulon, other regulators or enzymes may also be involved.

Isoniazid, targeting the mycobacterial enoyl reductase InhA, is one of the most potent TB drugs. Unfortunately, the progressive accumulation of isoniazid-resistant *M. tuberculosis* isolates seriously compromises the future of this antibiotic. Resistance to isoniazid is predominantly due to mutations in KatG, the catalase-peroxidase involved in the activation of this prodrug. As inhibiting mycobacterial enoyl reductase InhA is one of the most effective means of killing *M. tuberculosis*, important efforts have been developed to replace isoniazid with direct InhA inhibitors, but to date no orally active candidate has reached phase 2 clinical trials. An alternative to this approach would be the use of ETH to replace isoniazid. ETH is a prodrug also targeting InhA. In contrast to isoniazid, the activation of ETH in *M. tuberculosis* is independent of KatG, making this antibiotic fully active against isoniazid-resistant clinical isolates with mutations in the *katG* gene. In combination with moxifloxacine, ETH has been identified as an essential drug for the successful treatment of MDR-TB (*35*). Recent WHO guidelines recommended the inclusion of ETH in an all-oral shorter drug regimen for the treatment of MDR-TB where the injectable aminoglycoside agent is replaced by bedaquiline (*36*). Nevertheless, ETH has a less favorable therapeutic index than isoniazid because the dose required to inhibit *M. tuberculosis* growth sometimes causes adverse effects such as gastrointestinal disorders, hepatitis, and more rarely various mental disturbances (*37*, *38*).

It has been assumed that the activation of ETH is only achieved through the Baeyer-Villiger monooxygenase EthA (*7*–*9*), leading to the formation of a stable ETH-NAD adduct that inhibits the InhA of *M. tuberculosis* (*10*, *11*). As the production of EthA is regulated by the TetR-type transcriptional repressor EthR (*12*), we and others have successfully developed small-molecule inhibitors of EthR to stimulate the transcription of *ethA* (*13*–*15*, *18*, *22*), thus improving the activation of ETH and consequently its antibiotic activity (*19*). Recently, two additional regulons have been described to be able to participate in ETH activation, the regulon *Rv0077-Rv0078* (*ethA2-ethR2*) and the regulon *virS-mymA* encoding Rv3083 to Rv3089. Our group has shown that the small-molecule SMARt420 inhibits the transcriptional repressor Rv0078, stimulates the expression of the oxidoreductase Rv0077c, and restores the activation of ETH in clinical *M. tuberculosis* isolates with mutations in *ethA*. In the current study, we identified and developed a new series of compounds that stimulate the expression of the *mymA* operon. SMARt751, the best representative of this new compound series, showed potency in boosting ETH efficacy against a panel of MDR and XDR clinical isolates, including bacteria with mutations in *ethA* or the *inhA* promoter. Transcriptomics and quantitative proteomics showed that SMARt751 stimulated expression of all *mymA* operon genes and the respective proteins they encode. Moreover, SMARt751 also induced up-regulation of the *virS* gene, leading to overproduction of the VirS protein. The direct interaction between VirS and SMARt751 in vitro was shown by a thermal shift assay (Fig. 8, C and D). Using a mammalian reporter assay to eliminate the risk of VirS interacting with other mycobacterial proteins, we showed that the binding of VirS to the intergenic region between *virS* and *mymA* was impaired in the presence of SMARt751. These data suggested that the interaction of SMARt751 with VirS modulated the regulator function of VirS by impairing its DNA binding capacity. At the same time, treatment of bacteria with SMARt751 resulted in overexpression of the *mymA* operon. In light of previous reports showing that VirS acts as a transcriptional activator of *mymA* (*33*), the precise mechanism by which SMARt751 stimulates the expression of both *mymA* and *virS* remains to be elucidated.

Selection of *M. tuberculosis* mutants resistant to the ETH-SMARt751 combination pointed not only to MymA and VirS but also to Rv3080 (PknK), which modulates the expression of the *mymA* operon through phosphorylation of VirS (*39*). It has been reported that functional loss of *mymA* resulted in reduced ability of *M. tuberculosis* to persist in the spleen of infected guinea pigs (*34*). This suggests that mutations that inactivate the effect of SMARt751 may be counter-selected because of their impact on bacterial virulence. As observed in our transcriptomic data, SMARt751 also stimulated the expression of Rv0077c (EthA2), an enzyme that could participate in the efficacy of the ETH-SMARt751 combination and reversal of ETH resistance.

SMARt751 has a number of advantages. The mechanism by which it boosts the activity of ETH circumvents the most frequent mechanism of ETH resistance found in clinical isolates of *M. tuberculosis*, including mutations in *ethA*, the *ethR* promoter, and the *inhA* promoter. However, some attention will have to be paid to the *M. tuberculosis* sublineage 4.8 strain that harbors a large deletion covering the *virS-mymA* regulon (*40*). Treating chronically infected mice with an oral dose of 1 mg/kg of SMARt751 allowed a sixfold reduction in the effective plasma concentration of ETH. Furthermore, the observed efficacy of the ETH-SMARt751 combination against ETH-resistant *M. tuberculosis* in mice highlights the therapeutic potential of this combination in reversing ETH resistance in field isolates. The long-lasting effect of SMARt751 observed in vitro and in vivo suggests the potential of targeting transcriptional mechanisms and opens interesting avenues for the administration of similar compounds in humans. SMARt751 has shown no effect on the viability of the human HepG2 cell line in vitro, has not shown in vitro genetic toxicity, and has a low risk for arrhythmia. Effects of SMARt751 on mouse liver were recorded at doses higher than 20 mg/kg, suggesting reasonable

safety margins with respect to PK parameters in humans. Despite its high lipophilicity, SMARt751 displayed favorable PK properties after oral administration in mice and dogs. High oral doses in vivo (up to 200 mg/kg) were used in rat to counteract the expected first-pass metabolism of SMARt751 and achieve C_{max} and AUC values that would support evaluation of the safety window. Neither inhibition nor induction of the major CYP450 isoenzymes was observed in the preliminary study carried out in human microsomes and hepatocytes in vitro for the range of SMARt751 concentrations tested, suggesting a low risk of drug-drug interactions, which is an important consideration in the context of TB polytherapy and antiretroviral co-therapy. Regarding scalability of manufacturing, SMARt751 is a crystalline and low–molecular weight molecule that is prepared using a straightforward synthetic route. Last, SMARt751 also shows good penetration into cerebrospinal fluid. ETH is recommended in the treatment of drug-susceptible tuberculous meningitis (*41*); thus, the ETH-SMARt751 combination may be able to reduce side effects in the treatment of this deadliest form of TB.

Translating PK/PD data from in vitro cultures and animal models to predict an efficacious dose for humans remains a challenge and is obviously more complex when considering a combination of compounds. The new physiological-based PK modeling and simulation used here integrates the efficacy measurements of the ETH-SMARt751 combination in mice and the biotransformation and PK of both compounds and translates these parameters to human. The model predicts that as little as 25 mg/day (around 0.35 mg/kg) of SMARt751 would be sufficient to cut the efficacious dose of ETH in humans by fourfold. On the basis of existing clinical data, this would improve ETH tolerability. Therefore, the ETH-SMARt751 combination could be not only a second-line treatment for TB but also a possible substitute for the mycolic acid biosynthesis inhibitor isoniazid and part of a new first-line TB drug regimen.

MATERIALS AND METHODS

Study design

The objective of this study was the preclinical development of an N-acylated 4-phenylpiperidine small molecule that increased the sensitivity of *M. tuberculosis* to ETH and reversed resistance to ETH by altering the activation pathway of this antibiotic. The chemical structures of the rationally designed molecules synthesized and recrystallized in this study were confirmed by nuclear magnetic resonance (NMR) spectrometry. Thermostabilization of the putative targets—Rv3855 (EthR), Rv0078 (EthR2), and Rv3082c (VirS)—by these small molecules was measured using a thermal shift assay. The ability of these molecules to interfere with the binding of these three transcriptional regulators to their respective DNA operons was measured using a mammalian reporter assay. Their ability to boost ETH activity was quantified in axenic cultures of ETH-sensitive and ETH-resistant *M. tuberculosis* labeled with green fluorescent protein (GFP) and in cultures of infected macrophages. Chemical modifications performed to improve the metabolic stability of this small-molecule series led to development of the lead compound SMARt751.

Physicochemical properties and in vitro ADME were determined for SMARt751. In vivo drug metabolism and the PK profile of SMARt751 were investigated in three preclinical species: mouse, rat, and dog. Cytochrome P450 interactions and in vitro ADME were also studied in human hepatocyte cell cultures. Preliminary assessment of SMARt751 safety was investigated in pharmacology studies using hERG inhibition, off-target activity on 50 human targets, the ex vivo RVW model, electroencephalograms (EEGs), and behavioral end points in rats. Genetic toxicology was undertaken using the Ames test and mouse lymphoma assay (MLA), and an in vivo general toxicity study was conducted in mice. Animal experiments were performed in a fast-acute, an acute, and a chronic mouse model of tuberculosis. Selection of spontaneously resistant *M. tuberculosis* and transcriptomic and proteomic experiments confirmed the central role of the *virS-mymA* operon in the ability of SMARt751 to boost ETH activity.

Mice were purchased from Harlan Laboratories Inc. (The Netherlands) and randomly assigned to treatment groups. Detection of outliers was performed using the ROUT method with GraphPad Prism (maximum false discovery rate of $Q = 1\%$). Antibiotics were prepared and administered in a nonblinded fashion, both in vitro and in vivo. All animal studies were ethically reviewed and carried out in accordance with European Directive 2010/63/EU and the GSK Policy on the Care, Welfare and Treatment of Animals. All animal experimentation and procedures performed at Sciensano were validated and approved by the Ethical Committee of the IPH-VAR (Belgium) under the file number 120323-01. The animal facilities and procedures were under the supervision of an expert on animal welfare in accordance with the Belgian Ministry of Health.

M. tuberculosis ethA$^-$ E1 and H37Rv-GFP strains

The *M. tuberculosis* strain E1 is a derivative of the Beijing strain W4 that carries a $Gly^{343}Ala$ mutation in EthA, which causes resistance to ETH (MIC > 32 μg/ml measured by MGIT960). The recombinant strains of *M. tuberculosis* H37Rv expressing an enhanced GFP (H37Rv-GFP) were obtained by transformation of an integrative plasmid containing the Aequoria victoria egfp gene (*42*).

M. tuberculosis growth inhibition assay

ETH (Sigma-Aldrich, E6005-5G) was diluted in DMSO at 0.1 mg/ml, and aliquots were stored frozen at −20°C. Test compounds (booster candidates) were resuspended in DMSO at a concentration of 10 μM. ETH and test compounds were transferred to a 384-well low-volume polypropylene plate (Corning, no. 3672) and used to prepare assay plates. Briefly, 10 threefold serial dilutions of compounds were performed in black Greiner 384-well clear bottom polystyrene plates (Greiner, no. 781091) using an Echo 550 liquid handler (Labcyte). DMSO volume was compensated so that the concentrations across all wells were equal to 0.3%. Two independent replicates were made for each setting. Last, an equal volume of ETH (final concentration of 0.1 μg/ml for *M. tuberculosis*–GFP or 0.8 μg/ml for *M. tuberculosis*–GFP ethA$^-$) was dispensed into one of the replicates using Echo 550. On the day of the experiment, 50 μl of a culture of either *M. tuberculosis*–GFP H37Rv or *M. tuberculosis* E1-GFP (*ethA*$^-$) [OD_{600nm} (optical density at 600 nm) = 0.02] was transferred to each assay plate and incubated at 37°C for 5 days. The fluorescence intensity was measured at Ex/Em = 485/535 nm using the Victor Multilabel Plate Reader (PerkinElmer).

Long-lasting effect of SMARt751 on ETH activity in vitro and in vivo

H37Rv-GFP was diluted to an OD_{600nm} of 0.1 and treated with 1 μM SMARt751 24 hours before adding to assay plates containing a dose range of ETH or of ETH + 1 μM SMARt751. H37Rv-GFP was treated with DMSO and added to a dose range of ETH as control. Pretreated bacteria were centrifuged, washed twice with phosphate-buffered

saline (PBS), diluted in fresh culture medium to an OD_{600nm}, and transferred (50 µl) to assay plate, which were incubated at 37°C for 5 days. The fluorescence intensity was measured at Ex/Em = 485/535 nm using the Victor Multilabel Plate Reader (PerkinElmer). Microplates containing compound dilutions were prepared as described above.

The in vivo study was carried out similarly to the one described in the "in vivo mice fast-acute assay" except that ETH was administered on an "everyday schedule," whereas SMARt751 was given either every day, every 2 days (on days 1, 3, 5, and 7 after infection), or every 4 days (on days 1 and 5 after infection).

Ability of SMARt751 to induce cytochrome P450

Cryopreserved human hepatocytes were supplied by Triangle Research Laboratories and seeded according to the supplier's protocol in supplemented Williams E medium with serum. The hepatocytes were seeded on a 96-well collagen-coated plate at a density of 1×10^6 hepatocytes/ml (100 µl per well). The plate was incubated at 37°C for 4 hours before the seeding medium was replaced with 100 µl of supplemented Williams E medium without serum. The cells were cultured further for 24 hours before addition of the test compound in serum-free culture media (final test compound concentrations, 10, 4, 1, 0.4, 0.1, and 0.04 µM). Positive control inducers (omeprazole for CYP1A2, phenobarbital for CYP2B6, and rifampicin for CYP3A4) were incubated alongside the test compounds. Negative control wells were also included, where the test compound or positive control inducer was replaced by vehicle alone (0.1% DMSO in Williams E media for positive controls and test compound). The experiment was performed in triplicate. Upon completion of the 72-hour dosing period, the hepatocytes were washed twice with Williams E media. The hepatocytes were then lysed, and the lysate was stored at −80°C until the quantitative reverse transcription polymerase chain reaction (qRT-PCR) assay was performed. Total RNA was extracted from lysate, RNA quality and quantity were assessed, and reverse transcription was performed using the High-Capacity RNA-to-cDNA Kit (Applied Biosystems) and Veriti 96-Well Thermal Cycler (Applied Biosystems). Quantitative PCR analysis was performed on cDNA, using Applied Biosystems–designed TaqMan gene expression assays for the target genes CYP1A2, CYP2B6, CYP3A4, and endogenous control. Samples were analyzed using an ABI 7900 HT real-time PCR system. Relative fold mRNA expression level of the target genes was determined on the basis of the threshold cycle (CT) data of target gene relative to endogenous control for each reaction (ΔCT), normalized to the negative control (ΔΔCT). Fold induction was calculated using the $2^{-\Delta\Delta Ct}$ method. To determine whether the level of relative cytochrome P450 isoform mRNA expression was statistically different in the test compound samples compared to the appropriate negative controls, a one-way analysis of variance (ANOVA) with two-tailed Dunnett's posttest was performed. $P < 0.05$ was considered as the threshold for significance.

In vivo studies of SMARt751 PK

The PK and oral bioavailability of SMARt751 were investigated in mouse, rat, and dog after single intravenous and oral administration. To support efficacy studies, oral PK studies were also performed in female mice C57BL/6, the same strain used for efficacy model. To investigate in vivo CL and volume of distribution at steady state (Vss), intravenous PK studies were conducted in male CD-1 mice, male Sprague-Dawley rats, and male beagle dogs. Three animals per group were used for each study performed. A dose of 1 mg/kg was administered intravenously in a bolus form to mice and infused over a 30-min period to rats and dogs. For all the intravenous studies, compound was dissolved in 5% DMSO/20% Encapsin in saline. A dose of 5 mg/kg was orally administered by gavage to the rodent species, and a dose of 3 mg/kg was orally dosed to the dogs. In all the studies, SMARt751 was formulated as a suspension of 1% methylcellulose to investigate oral PK and to estimate oral bioavailability. Peripheral blood samples were obtained at 5, 15, and 30 min and 1, 2, 4, 6, 8, and 24 hours after intravenous administration in mice, 0.25, 0.5 (before end of infusion), 0.58, 0.75, 1, 1.5, 2, 3, 5, 7, and 24 hours after intravenous dosing in rats and dogs, and 0.25, 0.5, 0.75, 1, 2, 4, 6, 8, and 24 hours after oral administration for all the species. Blood was $^1/_2$ diluted with Milli-Q water and immediately frozen on dry ice until analysis. Quantification was performed by means of LC-MS/MS (API4000), with an LLOQ of 1 ng/ml. PK parameters, namely, CL, Vss, and bioavailability (F%), were estimated using Phoenix 64 (Pharsight, Certara).

Projection of human dosing for SMARt751

The human dose projections of SMARt751 and its estimated effect on the ETH dose reduction presented here are based on the semi-mechanistic mathematical PD model for TB established in (*31*) (also see fig. S9).

Preparation of *M. tuberculosis* genomic DNA

H37Rv spontaneous mutants to ETH-SMARt751 combinations were grown at 37°C until a saturated culture was obtained. One milliliter of saturated culture of each mutant was heat-inactivated for 30 min at 95°C. Total genomic DNA was extracted using a MasterPure DNA Purification kit (EpicentreBio, catalog no. MCD85201) according to the manufacturer's instructions. Briefly, bacterial pellets were collected by centrifugation, supernatant was discarded, and 25 µl of water was added. Pellets were vortexed briefly for 10 s. Then, 300 µl of lysis solution containing proteinase K was added and samples were mixed thoroughly. Samples were incubated at 65°C for 15 min with a brief vortex mix every 5 min. Samples were cooled to 37°C, and 1 µl of a ribonuclease A solution (5 µg/µl) was added to each sample, which were mixed thoroughly and incubated at 37°C for 30 min. Samples were cooled on ice for 5 min. DNA was precipitated by adding 175 µl of MPC Protein Precipitation Reagent (Epicentre) to 300 µl of lysed sample followed by vortexing for 10 s. Debris were pelleted by centrifugation at 4°C for 10 min at ≥10,000*g*. Supernatants were transferred to clean microcentrifuge tubes to which 500 µl of isopropanol was added. The tubes were inverted several times to mix well the two solutions. The DNA was collected by centrifugation at 4°C for 10 min at ≥10,000*g* and by carefully discarding the isopropanol. The DNA pellet was rinsed twice with 70% ethanol and resuspended in 35 µl of tris-EDTA buffer. DNA was quantified with a Qubit dsDNA HS Assay kit (Thermo Fisher Scientific) and sent to Fisabio (Valencia, Spain) for library preparation and whole-genome sequencing.

Transcriptomics analysis

M. tuberculosis H37Rv was grown at 37°C in 60-ml 7H9 supplemented with 2% (w/v) glucose and 0.025% (v/v) tyloxapol (Sigma-Aldrich) to an OD_{600nm} of 0.65. Ten 10 ml of culture were treated with each SMARt751 or DMSO to a final concentration of 10 µM or equivalent amount of DMSO. This procedure was done in triplicate. Incubation was continued for 24 hours at 37°C. Mycobacteria were

harvested by 10-min centrifugation at 5000*g* at 4°C, resuspended in 1 ml of RNApro (FastRNA Pro Blue Kit, MP Biomedicals), and homogenized in impact-resistant 2-ml tubes containing 0.1-mm silica spheres (Lysing Matrix B, MP Biomedicals) using a FastPrep FP120 cell disrupter (Thermo Fisher Scientific) at 6.0 Hz for 40 s. The ribolysed cells were centrifuged at 12,000*g* to remove cellular debris, and RNA was purified following the manufacturer's instructions. Ribosomal RNA (rRNA) depletion was performed using QIAseq FastSelect –5S/16S/23S Kits (Qiagen). Libraries for Illumina sequencing were prepared with the TruSeq RNA Sample Preparation Kit version 2.0 rev. A (Illumina Inc.). All cDNA libraries were uniquely indexed. cDNA libraries were sequenced using an Illumina NextSeq 500 system (Illumina Inc.) in high-output mode. All samples were multiplexed on one lane of the flow cell and sequenced in single-read sequencing mode with read lengths of 150 base pairs (bp). Raw RNA-seq reads were processed with Illumina quality control tools using default settings. Sequences shorter than 50 bp and/or that contained any "Ns" and/or with a mean quality score lower than 30 were removed using PRINSEQ (http://prinseq.sourceforge.net/index.html). Next, rRNA-specific reads were filtered out by mapping all the reads on *M. tuberculosis* rRNA sequences using Bowtie2 (http://bowtie-bio.sourceforge.net/bowtie2/index.shtml). Analysis of the RNA sequencing (RNA-seq) data was conducted using the SPARTA open-source software package with default parameters (https://sparta.readthedocs.io/en/latest/).

Proteomics analysis

Protein extraction

M. tuberculosis H37Rv was cultured in 7H9 medium without glycerol and supplemented with 2% (w/v) glucose and 0.025% (v/v) tyloxapol at 37°C for about 7 days until an OD_{600nm} of 0.8 was reached. The culture was diluted to an OD_{600nm} of 0.2, split in three subcultures. Two of them were further incubated for 72 hours in the presence of 1 μM SMARt751, and the third one was incubated with DMSO. Protein extracts were prepared by centrifuging the culture and washing the pellet with PBS before resuspending in 1 ml of lysis buffer [50 mM tris-HCl (pH 7.4), 0.8% (v/v) NP-40, 1.5 mM $MgCl_2$, 5% glycerol, 150 mM NaCl, 25 mM NaF, 1 mM Na_3VO_4, 1 mM dithiothreitol, and one cOmplete EDTA-free protease inhibitor tablet (Roche)], which was then disrupted using TissueLyser II (Qiagen) for three cycles at full amplitude for 5 min in refrigerated supports. Bacterial lysates were centrifuged at 14,000*g* for 30 min, and the supernatant was filtered using Millex LG (PTFE) 0.2 μm/13 mm diameter. Filtered supernatants were further ultracentrifuged at 4°C for 60 min (140,000*g*). Samples were prepared in quadruplicate.

Chemoproteomics methods

SDS sample buffer (2% SDS, 10% glycerol, 0.005% bromophenol blue, 100 mM tris-HCl, and 125 mM tris base) was added to 37.5 μl of the *M. tuberculosis* protein extract. The contained proteins were digested according to a modified single-pot solid-phase sample preparation (SP3) protocol (*43*, *44*) described in Supplementary Materials and Methods.

Toxicology and safety pharmacology studies

Ames (*45*) and MLA mutagenicity assays (*46*), the hERG assay (*45*), QT interval evaluation (*47*), and the arterially perfused RVW assay (*47*) were performed as described previously.

Rat EEG was used to evaluate the activity SMARt751 after a single administration at 100 mg/kg of body weight and 300 mg/kg of body weight and after the repeated administration, over 7 days, at 300 mg/kg of body weight, on the EEG parameters by EEG trace monitoring in male Crl:WI(Han) rats (*48*).

Mouse 4-day toxicology of SMARt751 was evaluated on male Crl:CD1(ICR) mice (six per group) at doses of 0 (vehicle), 20, 60, or 200 mg/kg of body weight/day once daily for 4 days by oral gavage at a dose volume of 10 ml/kg of body weight. Six additional males were added to the 60 mg/kg of body weight/day dose group and were dosed for 4 days to assess brain concentration compared to blood concentration. The following end points/parameters were evaluated: clinical observations, body weights, limited clinical chemistry results, organ weights (liver including gall bladder, brain, heart, kidneys, and testes), and macroscopic and microscopic observations (heart, kidneys, mesenteric lymph node, skeletal muscle, testes, liver, and gall bladder). Toxicokinetic (composite) evaluation was performed on samples collected from SMARt751-dosed animals on days 1 and 4. Brain tissue and blood samples from animals given 60 mg/kg of body weight/day were analyzed for SMARt751 concentration on day 4 (three males per time point at 0.5, 3, and 24 hours after dosing).

Statistics

In vitro data are presented as means ± SD of biological replicates. Raw data of in vitro and in vivo experiments are listed in data file S1. Fitting for all in vivo experiments was done using GraphPad Prism v9. For the fast-acute and the chronic in vivo mouse models of *M. tuberculosis* infection, nonlinear fitting to logistic equation of $\log_{10}$ versus dose was used to fit the curve (sigmoidal response curve; variable slope) and obtain 95% CI. Experiments were repeated a minimum of three times. For the in vivo experiment showing the long-lasting boosting effect of SMARt751 on ETH (Fig. 3B), comparison between groups was done using Dunnett's multiple comparisons test. $P < 0.05$ was considered to be statistically significant. For the mouse experiment measuring the efficacy of SMARt751 treatment on the ETH-resistant strain E1 (Fig. 6), comparison between groups was done using Bonferroni's multiple comparisons test. $P < 0.05$ was considered to be statistically significant. Graphs for in vivo experiments indicate the limit of detection. Transcriptomic experiments were done on biological triplicates. Analysis of the RNA-seq data was conducted using the SPARTA open-source software package with default parameters. Differential gene expression analysis was performed using EdgeR (https://sparta.readthedocs.io/en/latest/). Figure 8A and table S7 report means of fold changes and *P* values for genes where transcription was increased or decreased more than threefold. Raw transcriptomic data are available in data file S1. Proteomics was performed on biological duplicates (Fig. 8B). Single spectrum to sequence assignments was attributed to best match with a minimum Mascot score of 31 and a 10× difference of this assignment over the next best assignment. Quantified proteins were required to contain at least two unique peptide matches.

SUPPLEMENTARY MATERIALS

www.science.org/doi/10.1126/scitranslmed.aaz6280
Materials and Methods
Figs. S1 to S11
Tables S1 to S7
Data file S1
References (*49*–*54*)

View/request a protocol for this paper from *Bio-protocol*.

REFERENCES AND NOTES

1. World Health Organization, "Global Tuberculosis Report 2021" (World Health Organization, 2021).
2. M. Uplekar, D. Weil, K. Lonnroth, E. Jaramillo, C. Lienhardt, H. M. Dias, D. Falzon, K. Floyd, G. Gargioni, H. Getahun, C. Gilpin, P. Glaziou, M. Grzemska, F. Mirzayev, H. Nakatani, M. Raviglione, WHO's new end TB strategy. *Lancet* **385**, 1799–1801 (2015).
3. M. L. Bastos, Z. Lan, D. Menzies, An updated systematic review and meta-analysis for treatment of multidrug-resistant tuberculosis. *Eur. Respir. J.* **49**, 1600803 (2017).
4. J. Laborde, C. Deraeve, V. Bernardes-Genisson, Update of antitubercular prodrugs from a molecular perspective: Mechanisms of action, Bioactivation pathways, and associated resistance. *ChemMedChem* **12**, 1657–1676 (2017).
5. T. Yano, S. Kassovska-Bratinova, J. S. Teh, J. Winkler, K. Sullivan, A. Isaacs, N. M. Schechter, H. Rubin, Reduction of clofazimine by mycobacterial type 2 NADH:quinone oxidoreductase: A pathway for the generation of bactericidal levels of reactive oxygen species. *J. Biol. Chem.* **286**, 10276–10287 (2011).
6. A. M. Upton, S. Cho, T. J. Yang, Y. Kim, Y. Wang, Y. Lu, B. Wang, J. Xu, K. Mdluli, Z. Ma, S. G. Franzblau, In vitro and in vivo activities of the nitroimidazole TBA-354 against mycobacterium tuberculosis. *Antimicrob. Agents Chemother.* **59**, 136–144 (2015).
7. T. A. Vannelli, A. Dykman, P. R. Ortiz De Montellano, The antituberculosis drug ethionamide is activated by a flavoprotein monooxygenase. *J. Biol. Chem.* **277**, 12824–12829 (2002).
8. A. R. Baulard, J. C. Betts, J. Engohang-Ndong, S. Quan, R. A. McAdam, P. J. Brennan, C. Locht, G. S. Besra, Activation of the pro-drug ethionamide is regulated in mycobacteria. *J. Biol. Chem.* **275**, 28326–28331 (2000).
9. A. E. DeBarber, K. Mdluli, M. Bosman, L. G. Bekker, C. E. Barry 3rd, Ethionamide activation and sensitivity in multidrug-resistant *Mycobacterium tuberculosis*. *Proc. Natl. Acad. Sci. U.S.A.* **97**, 9677–9682 (2000).
10. F. Wang, R. Langley, G. Gulten, L. G. Dover, G. S. Besra, W. R. Jacobs Jr., J. C. Sacchettini, Mechanism of thioamide drug action against tuberculosis and leprosy. *J. Exp. Med.* **204**, 73–78 (2007).
11. A. Banerjee, E. Dubnau, A. Quemard, V. Balasubramanian, K. S. Um, T. Wilson, D. Collins, G. Delisle, W. R. Jacobs, *inhA*, a gene encoding a target for isoniazid and ethionamide in *Mycobacterium tuberculosis*. *Science* **263**, 227–230 (1994).
12. J. Engohang-Ndong, D. Baillat, M. Aumercier, F. Bellefontaine, G. S. Besra, C. Locht, A. R. Baulard, EthR, a repressor of the TetR/CamR family implicated in ethionamide resistance in mycobacteria, octamerizes cooperatively on its operator. *Mol. Microbiol.* **51**, 175–188 (2004).
13. M. Flipo, M. Desroses, N. Lecat-Guillet, B. Dirié, X. Carette, F. Leroux, C. Piveteau, F. Demirkaya, Z. Lens, P. Rucktooa, V. Villeret, T. Christophe, H. K. Jeon, C. Locht, P. Brodin, B. Déprez, A. R. Baulard, N. Willand, Ethionamide boosters: Synthesis, biological activity, and structure-activity relationships of a series of 1,2,4-oxadiazole EthR inhibitors. *J. Med. Chem.* **54**, 2994–3010 (2011).
14. M. Flipo, M. Desroses, N. Lecat-Guillet, B. Villemagne, N. Blondiaux, F. Leroux, C. Piveteau, V. Mathys, M. P. Flament, J. Siepmann, V. Villeret, A. Wohlkonig, R. Wintjens, S. H. Soror, T. Christophe, H. K. Jeon, C. Locht, P. Brodin, B. Deprez, A. R. Baulard, N. Willand, Ethionamide boosters. 2. Combining bioisosteric replacement and structure-based drug design to solve pharmacokinetic issues in a series of potent 1,2,4-oxadiazole EthR inhibitors. *J. Med. Chem.* **55**, 68–83 (2012).
15. M. Flipo, N. Willand, N. Lecat-Guillet, C. Hounsou, M. Desroses, F. Leroux, Z. Lens, V. Villeret, A. Wohlkonig, R. Wintjens, T. Christophe, H. Kyoung Jeon, C. Locht, P. Brodin, A. R. Baulard, B. Deprez, Discovery of novel N-phenylphenoxyacetamide derivatives as EthR inhibitors and ethionamide boosters by combining high-throughput screening and synthesis. *J. Med. Chem.* **55**, 6391–6402 (2012).
16. N. J. Tatum, J. W. Liebeschuetz, J. C. Cole, R. Frita, A. Herledan, A. R. Baulard, N. Willand, E. Pohl, New active leads for tuberculosis booster drugs by structure-based drug discovery. *Org. Biomol. Chem.* **15**, 10245–10255 (2017).
17. B. Villemagne, A. MacHelart, N. C. Tran, M. Flipo, M. Moune, F. Leroux, C. Piveteau, A. Wohlkönig, R. Wintjens, X. Li, R. Gref, P. Brodin, B. Deprez, A. R. Baulard, N. Willand, Fragment-based optimized EthR inhibitors with in vivo ethionamide boosting activity. *ACS Infect. Dis.* **6**, 366–378 (2020).
18. N. Willand, M. Desroses, P. Toto, B. Dirié, Z. Lens, V. Villeret, P. Rucktooa, C. Locht, A. Baulard, B. Deprez, Exploring drug target flexibility using in situ click chemistry: Application to a mycobacterial transcriptional regulator. *ACS Chem. Biol.* **5**, 1007–1013 (2010).
19. N. Willand, B. Dirié, X. Carette, P. Bifani, A. Singhal, M. Desroses, F. Leroux, E. Willery, V. Mathys, R. Déprez-Poulain, G. Delcroix, F. Frénois, M. Aumercier, C. Locht, V. Villeret, B. Déprez, A. R. Baulard, Synthetic EthR inhibitors boost antituberculous activity of ethionamide. *Nat. Med.* **15**, 537–544 (2009).
20. N. Willand, M. Flipo, B. Villemagne, A. Baulard, B. Deprez, Recent advances in the design of inhibitors of mycobacterial transcriptional regulators to boost thioamides anti-tubercular activity and circumvent acquired-resistance. *Annu. Rep. Med. Chem.* **52**, 131–152 (2019).
21. P. O. Nikiforov, M. Blaszczyk, S. Surade, H. I. Boshoff, A. Sajid, V. Delorme, N. Deboosere, P. Brodin, A. R. Baulard, C. E. Barry Rd, T. L. Blundell, C. Abell, Fragment-sized EthR inhibitors exhibit exceptionally strong ethionamide boosting effect in whole cell *Mycobacterium tuberculosis* assays. *ACS Chem. Biol.* **12**, 1390–1396 (2017).
22. P. O. Nikiforov, S. Surade, M. Blaszczyk, V. Delorme, P. Brodin, A. R. Baulard, T. L. Blundell, C. Abell, A fragment merging approach towards the development of small molecule inhibitors of Mycobacterium tuberculosis EthR for use as ethionamide boosters. *Org. Biomol. Chem.* **14**, 2318–2326 (2016).
23. F. Frénois, J. Engohang-Ndong, C. Locht, A. R. Baulard, V. Villeret, Structure of EthR in a ligand bound conformation reveals therapeutic perspectives against tuberculosis. *Mol. Cell* **16**, 301–307 (2004).
24. N. Blondiaux, M. Moune, M. Desroses, R. Frita, M. Flipo, V. Mathys, K. Soetaert, M. Kiass, V. Delorme, K. Djaout, V. Trebosc, C. Kemmer, R. Wintjens, A. Wohlkonig, R. Antoine, L. Huot, D. Hot, M. Coscolla, J. Feldmann, S. Gagneux, C. Locht, P. Brodin, M. Gitzinger, B. Deprez, N. Willand, A. R. Baulard, Reversion of antibiotic resistance Mycobacterium tuberculosis by spiroisoxazoline SMARt-420. *Science* **355**, 1206–1211 (2017).
25. S. S. Grant, S. Wellington, T. Kawate, C. A. Desjardins, M. R. Silvis, C. Wivagg, M. Thompson, K. Gordon, E. Kazyanskaya, R. Nietupski, N. Haseley, N. Iwase, A. M. Earl, M. Fitzgerald, D. T. Hung, Baeyer-villiger monooxygenases EthA and MymA are required for activation of replicating and non-replicating mycobacterium tuberculosis inhibitors. *Cell Chem. Biol.* **23**, 666–677 (2016).
26. J. Rullas, J. I. Garcia, M. Beltran, P. J. Cardona, N. Caceres, J. F. Garcia-Bustos, I. Angulo-Barturen, Fast standardized therapeutic-efficacy assay for drug discovery against tuberculosis. *Antimicrob. Agents Chemother.* **54**, 2262–2264 (2010).
27. M. Zhu, R. Namdar, J. J. Stambaugh, J. R. Starke, A. E. Bulpitt, S. E. Berning, C. A. Peloquin, Population pharmacokinetics of ethionamide in patients with tuberculosis. *Tuberculosis* **82**, 91–96 (2002).
28. S. Thee, H. I. Seifart, B. Rosenkranz, A. C. Hesseling, K. Magdorf, P. R. Donald, H. S. Schaaf, Pharmacokinetics of ethionamide in children. *Antimicrob. Agents Chemother.* **55**, 4594–4600 (2011).
29. C. Vilcheze, W. R. Jacobs Jr., Resistance to isoniazid and ethionamide in mycobacterium tuberculosis: Genes, mutations, and causalities. *Microbiol. Spectr.* **2**, MGM2-0014-2013 (2014).
30. R. P. Dash, R. Jayachandra Babu, N. R. Srinivas, Therapeutic potential and utility of elacridar with respect to P-glycoprotein inhibition: An insight from the published in vitro, preclinical and clinical studies. *Eur. J. Drug Metab. Pharmacokinet.* **42**, 915–933 (2017).
31. M. Muliaditan, O. Della Pasqua, Model-based rationale for drug combinations in tuberculosis. *Abstr. Annu. Meet. Popul. Approach Group Europe* **Abstr 7272**, 26 (2017).
32. W. S. Redfern, L. Carlsson, A. S. Davis, W. G. Lynch, I. MacKenzie, S. Palethorpe, P. K. Siegl, I. Strang, A. T. Sullivan, R. Wallis, A. J. Camm, T. G. Hammond, Relationships between preclinical cardiac electrophysiology, clinical QT interval prolongation and torsade de pointes for a broad range of drugs: Evidence for a provisional safety margin in drug development. *Cardiovasc. Res.* **58**, 32–45 (2003).
33. A. Singh, S. Jain, S. Gupta, T. Das, A. K. Tyagi, mymA operon of Mycobacterium tuberculosis: Its regulation and importance in the cell envelope. *FEMS Microbiol. Lett.* **227**, 53–63 (2003).
34. A. Singh, R. Gupta, R. A. Vishwakarma, P. R. Narayanan, C. N. Paramasivan, V. D. Ramanathan, A. K. Tyagi, Requirement of the mymA operon for appropriate cell wall ultrastructure and persistence of mycobacterium tuberculosis in the spleens of guinea pigs. *J. Bacteriol.* **187**, 4173–4186 (2005).
35. S. D. Ahuja, D. Ashkin, M. Avendano, R. Banerjee, M. Bauer, J. N. Bayona, M. C. Becerra, A. Benedetti, M. Burgos, R. Centis, E. D. Chan, C. Y. Chiang, H. Cox, L. D'Ambrosio, K. DeRiemer, N. H. Dung, D. Enarson, D. Falzon, K. Flanagan, J. Flood, M. L. Garcia-Garcia, N. Gandhi, R. M. Granich, M. G. Hollm-Delgado, T. H. Holtz, M. D. Iseman, L. G. Jarlsberg, S. Keshavjee, H. R. Kim, W. J. Koh, J. Lancaster, C. Lange, W. C. de Lange, V. Leimane, C. C. Leung, J. Li, D. Menzies, G. B. Migliori, S. P. Mishustin, C. D. Mitnick, M. Narita, P. O'Riordan, M. Pai, D. Palmero, S. K. Park, G. Pasvol, J. Pena, C. Perez-Guzman, M. I. Quelapio, A. Ponce-de-Leon, V. Riekstina, J. Robert, S. Royce, H. S. Schaaf, K. J. Seung, L. Shah, T. S. Shim, S. S. Shin, Y. Shiraishi, J. Sifuentes-Osornio, G. Sotgiu, M. J. Strand, P. Tabarsi, T. E. Tupasi, R. van Altena, M. Van der Walt, T. S. Van der Werf, M. H. Vargas, P. Viiklepp, J. Westenhouse, W. W. Yew, J. J. Yim, Multidrug resistant pulmonary tuberculosis treatment regimens and patient outcomes: An individual patient data meta-analysis of 9,153 patients. *PLOS Med.* **9**, e1001300 (2012).
36. World Health Organization, *WHO Consolidated Guidelines on Tuberculosis: Module 4: Treatment - Drug-Resistant Tuberculosis Treatment* (World Health Organization, 2020).
37. D. K. Gupta, O. P. Mital, M. C. Agarwal, H. M. Kansal, S. Nath, A comparison of therapeutic efficacy and toxicity of ethionamide and prothionamide in Indian patients. *J. Indian Med. Assoc.* **68**, 25–29 (1977).

38. E. Tala, K. Tevola, Side effects and toxicity of ethionamide and prothionamide. *Ann. Clin. Res.* **1**, 32–35 (1969).
39. P. Kumar, D. Kumar, A. Parikh, D. Rananaware, M. Gupta, Y. Singh, V. K. Nandicoori, The Mycobacterium tuberculosis protein kinase K modulates activation of transcription from the promoter of mycobacterial monooxygenase operon through phosphorylation of the transcriptional regulator VirS. *J. Biol. Chem.* **284**, 11090–11099 (2009).
40. A. G. Tsolaki, A. E. Hirsh, K. DeRiemer, J. A. Enciso, M. Z. Wong, M. Hannan, Y. O. G. de la Salmoniere, K. Aman, M. Kato-Maeda, P. M. Small, Functional and evolutionary genomics of Mycobacterium tuberculosis: Insights from genomic deletions in 100 strains. *Proc. Natl. Acad. Sci. U.S.A.* **101**, 4865–4870 (2004).
41. P. R. Donald, Cerebrospinal fluid concentrations of antituberculosis agents in adults and children. *Tuberculosis* **90**, 279–292 (2010).
42. V. Delorme, O. R. Song, A. Baulard, P. Brodin, Testing chemical and genetic Modulators in Mycobacterium tuberculosis infected cells using phenotypic assays. *Methods Mol. Biol.* **1285**, 387–411 (2015).
43. C. S. Hughes, S. Foehr, D. A. Garfield, E. E. Furlong, L. M. Steinmetz, J. Krijgsveld, Ultrasensitive proteome analysis using paramagnetic bead technology. *Mol. Syst. Biol.* **10**, 757 (2014).
44. S. Moggridge, P. H. Sorensen, G. B. Morin, C. S. Hughes, Extending the compatibility of the SP3 paramagnetic bead processing approach for proteomics. *J. Proteome Res.* **17**, 1730–1740 (2018).
45. B. N. Ames, J. McCann, E. Yamasaki, Methods for detecting carcinogens and mutagens with the Salmonella/mammalian-microsome mutagenicity test. *Mutat. Res.* **31**, 347–363 (1975).
46. D. Clive, K. O. Johnson, J. F. Spector, A. G. Batson, M. M. Brown, Validation and characterization of the L5178Y/TK+/− mouse lymphoma mutagen assay system. *Mutat. Res.* **59**, 61–108 (1979).
47. R. R. Shah, Drug-induced QT interval shortening: Potential harbinger of proarrhythmia and regulatory perspectives. *Br. J. Pharmacol.* **159**, 58–69 (2010).
48. N. Durmuller, R. D. Porsolt, R. Scherschlicht, Vigilance-controlled quantified EEG in safety pharmacology. *Curr. Protoc. Pharmacol.* **11**, 10.16.11–10.16.27 (2001).
49. M. Martinez-Hoyos, E. Perez-Herran, G. Gulten, L. Encinas, D. Alvarez-Gomez, E. Alvarez, S. Ferrer-Bazaga, A. G.-Perez, F. Ortega, I. A.-Barturen, J. Rullas-Trincado, D. B. Ruano, P. Torres, P. Castaneda, S. Huss, R. F. Menendez, S. G. Del Valle, L. Ballell, D. Barros, S. Modha, N. Dhar, F. S.-Gelo, J. D. McKinney, J. F. G.-Bustos, J. L. Lavandera, J. C. Sacchettini, M. S. Jimenez, N. Martin-Casabona, J. Castro-Pichel, A. Mendoza-Losana, Antitubercular drugs for an old target: GSK693 as a promising InhA direct inhibitor. *EBioMedicine* **8**, 291–301 (2016).
50. S. Singh, N. Goswami, A. K. Tyagi, G. Khare, Unraveling the role of the transcriptional regulator VirS in low pH–induced responses of Mycobacterium tuberculosis and identification of VirS inhibitors. *J. Biol. Chem.* **294**, 10055–10075 (2019).
51. S. Schlatter, M. Rimann, J. Kelm, M. Fussenegger, SAMY, a novel mammalian reporter gene derived from Bacillus stearothermophilus alpha-amylase. *Gene* **282**, 19–31 (2002).
52. T. Werner, I. Becher, G. Sweetman, C. Doce, M. M. Savitski, M. Bantscheff, High-resolution enabled TMT 8-plexing. *Anal. Chem.* **84**, 7188–7194 (2012).
53. T. Werner, G. Sweetman, M. F. Savitski, T. Mathieson, M. Bantscheff, M. M. Savitski, Ion coalescence of neutron encoded TMT 10-plex reporter ions. *Anal. Chem.* **86**, 3594–3601 (2014).
54. The MathWorks Inc., MATLAB and SimBiology Toolbox Release 2018b.
55. C. A. Lipinski, F. Lombardo, B. W. Dominy, P. J. Feeney, Experimental and computational approaches to estimate solubility and permeability in drug discovery and development settings. *Adv. Drug Deliv. Rev.* **46**, 3–26 (2001).

Acknowledgments: We thank D. Hung (Broad Institute) for transposon mutants Rv3854c::Tn and Rv3083::Tn and clone 3RM4. We also thank F. J. Gamo, N. Cammack, A. Tartar, M. Turner, F. J. Gamo, and C. Locht for their scientific input or support, as well as R. Frères for the gift of Kleptose HP. We thank ARIADNE-criblage (UMS2014-UAR2014-PLBS) and ARIADNE-ADME (French national infrastructure ChemBioFrance) for providing access to their facilities and procedures. **Funding:** This work was supported by l'Agence Nationale de la Recherche (ANR), France (Tea-4-Two/ANR-14-CE14-0027-01 and Equipex Imaginex BioMed/ANR-10-EQPX-04-01 to A.R.B. and N.W.), EU grants ERC-STG INTRACELL-TB n° 260901 and the Feder (12001407 (D-AL) to P.B. and V.D., SATT-Nord (TB-Boost project) to A.R.B. and N.W., and INSERM, Université de Lille, Institut Pasteur de Lille, CNRS, Région Hauts-de-France to M.F., R.F., M. Bourotte, F.L. C.P., R.A., P.B., V.D., K.D., S.S., B.D., N.W., and A.R.B. This work was also funded by Bioversys and GlaxoSmithKline. R.W. is a Research Associate with the Belgian National Funds for Scientific Research (FRS-FNRS). This work was also funded by Bioversys, the Wellcome Trust and GlaxoSmithKline. **Author contributions:** M.F. designed the arylpiperidine series and SMARt751. R.F. performed molecular biology experiments and axenic MIC. M. Bourotte performed synthesis of compounds and analyzed data. M.S.M.-M. designed DMPK experiments and performed human PK estimation. M. Boesche performed mass spectrometry. G.W.B. designed DMPK experiments. G. Derimanov contributed to the design of toxicology experiments. G. Drewes and S.G.-D. designed mass spectrometry experiments and analyzed data. P.G. performed PD modeling. S.G. and E.J. designed safety experiments. J.d.M. performed DMPK analysis. E.P.-H. designed and performed in vitro experiments. E.P.-D.F. contributed to the design of in vitro experiments and data analysis. J.R. designed in vivo experiments. P.C. performed statistics on data from in vivo experiments. F.L. designed eADME experiments and analyzed data. C.P. performed LC-MS and eADME experiments. M.K. performed in vivo experiments in the chronic TB mouse model and analyzed data. V. Mathys performed in vitro evaluation of the compounds and in vivo experiments. K.S. performed in vitro experiments on clinical isolates. V. Megalizzi performed thermal shift assays on VirS. A.T. purified VirS. R.W. designed TSA experiments on VirS and analyzed data. R.A. designed and analyzed transcriptomics data. V.D. performed axenic MIC experiments with H37Rv-GFP, and P.B. analyzed these data. M.M. performed molecular biology experiments. K.D. and S.S. performed transcriptomic experiments and analyzed data. C.K. performed mammalian assay experiments. A.M.-L., M.G., L.B., S.L., B.D., D.B.A., M.J.R., N.W., and A.R.B. performed data analysis and led all studies. A.R.B. drafted the manuscript, and M.F., R.F., M.S.M.-M., G.W.B., G. Derimanov, G. Drewes, P.G., S.G.-D., S.G., J.R., R.W., B.D., M.J.R., and N.W. contributed to the writing of the manuscript. **Competing interests:** M. Boesche, M.G., S.L., and C.K. are Bioversys employees. C.K., S.L., and M.G. own shares of Bioversys. N.W., B.D., A.R.B., P.B., and M.F. are listed as co-inventors on patent no. FR3000065A1 (WO2014096378) entitled "Bicyclic compounds having an activity potentiating the activity of an antibiotic active against mycobacteria—composition and pharmaceutical product comprising such compounds." A.R.B. and N.W. are consultants for Bioversys. B.D. is paid as scientific co-director of Institut Pasteur de Lille. The other authors declare that they have no competing interests. **Data and materials availability:** All data associated with this study are present in the paper or the Supplementary Materials. SMARt compounds and *M. tuberculosis* clones listed in this manuscript are available from A. Baulard or N. Willand under a materials transfer agreement with Institut Pasteur de Lille. The *M. tuberculosis* clinical isolates described in table S1 are available from V. Mathys under a materials transfer agreement with Sciensano.

Submitted 25 September 2019
Resubmitted 12 April 2021
Accepted 4 October 2021
Published 4 May 2022
10.1126/scitranslmed.aaz6280

Abstract

One-sentence summary: The small-molecule SMARt751 reverses *M. tuberculosis* resistance to ethionamide by up-regulating the *mymA* operon.

Editor's Summary:
Boosting the action of a TB drug

Tuberculosis (TB) is an infectious disease caused by *Mycobacterium tuberculosis* and is one of the leading causes of death from a single infectious agent. Ethionamide is a prodrug used to treat multidrug resistant TB. MymA is a mycobacterial oxidase that is responsible for the activation of ethionamide. The production of MymA is under the control of the transcriptional regulator VirS. Flipo *et al.* now report the discovery of the small-molecule SMARt751, a VirS ligand that up-regulates expression of the *mymA* operon. SMARt751 reversed resistance to ethionamide in mouse models of acute and chronic TB.